CONTINUATION OF QUASI-PERIODIC INVARIANT TORI

FRANK SCHILDER*, HINKE M. OSINGA*, AND WERNER VOGT**

Abstract. Many systems in science and engineering can be modelled as coupled or forced nonlinear oscillators which may possess quasi-periodic or phase-locked invariant tori. Since there exist routes to chaos involving the break-down of invariant tori, these phenomena attract considerable attention. After a brief historical overview of known methods for the computation of invariant tori this paper presents a new algorithm for the computation and continuation of quasi-periodic invariant tori of ordinary differential equations.

The proposed algorithm is based on a novel invariance equation which gives rise to a natural parametrisation of quasi-periodic invariant tori. The discretisation of this invariance equation gives an algorithm that is easy to implement and immediately suitable for continuation. Consistency and stability of a finite-difference discretisation is shown in the case that the differential equation can be written in generalised radius-angle coordinates.

Since the parametrisation is uniquely defined, the proposed method requires neither the computation of a base of a transversal bundle, nor re-meshing during continuation, but uses only information in the tangent space of a torus. It is independent of the stability type of the torus and examples of attracting and saddle-type tori are given. The algorithm is robust in the sense that it can compute reliable approximations to weakly resonant tori. The performance of our method is demonstrated with extensive examples.

Key words. invariant tori, continuation, invariance condition, finite-difference method

AMS subject classifications. 37M99 (37D10, 37M20, 65L99, 65P05)

1. Introduction. Coupled or forced oscillators occur in many applications as far ranging as aerodynamics and chemical reactions; we refer, for example, to [27] as an entry point to the extensive literature. These oscillators can exhibit quasi-periodic oscillations, that is, oscillations with at least two (incommensurate) internal frequencies [8, 49]. Recent fields of applications in which quasi-periodic oscillations were reported include laser dynamics [3, 37, 38], rotor dynamics of jet engines [5], power networks [14, 32] and population dynamics in chemostats [39].

A quasi-periodic oscillation (motion) takes place on a quasi-periodic invariant torus which is densely filled by quasi-periodic orbits [8, 49]. In this paper we consider the computation of such a quasi-periodic invariant torus of an ordinary differential equation (ODE)

$$\dot{x} = f(x,\lambda)\,, \qquad f : \mathbb{R}^n \times \mathbb{R}^m \to \mathbb{R}^n\,,\ \ n \geq 3\,,\ \ m \geq 0\,. \tag{1.1}$$

Here $\lambda \in \mathbb{R}^m$ is a parameter and we always assume that f is sufficiently smooth. Whenever the dependence on λ is not relevant, for example, when λ is constant, we omit the explicit argument λ for simplicity. In addition, we suppose that (1.1) has a quasi-periodic invariant torus for some λ_0. Note that a quasi-periodic invariant torus is as smooth as the flow generated by (1.1) [49]. Since the right-hand side of (1.1) depends on an external parameter λ, one may also be interested in parameter continuation, that is, the computation of a family of invariant quasi-periodic tori. In this context, the question of persistence of quasi-periodic invariant tori becomes important.

*Bristol Centre for Applied Nonlinear Mathematics, Department of Engineering Mathematics, University of Bristol, Bristol BS8 1TR, UK.

**Technical University of Ilmenau, Department of Numerical Analysis, Post-box 100565, 98684 Ilmenau, Germany.

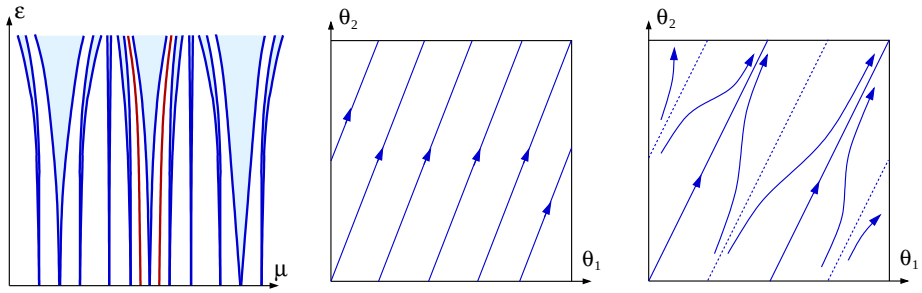

(a) (b) (c)

FIGURE 1.1. *Sketch of Arnol′d tongues in a two-dimensional parameter space* (*a*). *In between the Arnol′d tongues exists continuous curves* (*red*), *where the flow on the torus is quasi-periodic. Panels* (*b*) *and* (*c*) *show parallel and phase-locked flow, respectively, on the two dimensional standard torus.*

Typically, an invariant quasi-periodic torus persists as a differentiable manifold under small perturbations because it is *normally hyperbolic*. This means that the attraction (expansion) transverse to the torus is stronger than the attraction (expansion) on the torus; see [24, 53] for the precise formulation of normal hyperbolicity and [8] for how it can be expressed in terms of a Floquet form. However, the flow on the torus may change from quasi-periodic to phase-locked after which normal hyperbolicity may be lost such that the torus is destroyed.

Let us, for the moment, assume that (1.1) has a quasi-periodic invariant 2-torus and depends on two parameters $\lambda = (\mu, \varepsilon)$ such that for $\varepsilon = 0$ the flow on the torus is diffeomorphic to a parallel flow; see Fig. 1.1 (b). Then Fig. 1.1 illustrates the typical behaviour of the flow on an invariant torus as the parameters change; see also [2, 8, 26, 27].

For small $\varepsilon > 0$ the parameter space features so-called Arnol′d tongues as is sketched in Fig. 1.1 (a). For parameter values inside an Arnol′d tongue the flow on the torus is phase-locked, that is, a stable and an unstable periodic orbit exists on the torus and the flow is not diffeomorphic to a parallel flow; see Fig. 1.1 (c). In between the Arnol′d tongues there exist continuous curves where the flow is quasi-periodic. These curves are of finite length and end at points where neighbouring Arnol′d tongues start to overlap [45]. Thus, quasi-periodic invariant tori exist for parameter values in a Cantor set of positive measure. Such a family of quasi-periodic invariant tori is also called a *Cantor-like family* [8]. Note that there exists an open set of parameter values such that the Arnol′d tongues do not overlap. Invariant tori may exist for parameter values in this set.

In this paper we propose a *natural parametrisation* of a quasi-periodic invariant torus which is obtained by using a novel invariance equation; see §3. An easy-to-implement algorithm is derived by discretising this invariance equation by using finite-differences. This discretisation can be constructed by recursion over the dimension p of the torus; see §4.4. Therefore, our implementation can be used for the computation of quasi-periodic invariant tori of arbitrary fixed dimension p, the limiting factor being only the available computational power. A proof of consistency and stability is given in §4.2 for the case that the ODE (1.1) is available in a partitioned form, meaning that it can be written in generalised radius-angle coordinates; see §2.2 for more details.

Since the parametrisation is uniquely defined, the proposed method requires

neither the computation of a base of a transversal bundle, nor re-meshing during continuation, it uses only information in the tangent space of a torus. Thus, it is naturally suited for continuation and is incorporated into a one-parameter pseudo-arc-length continuation algorithm. Even though the derivation of the algorithm applies to the quasi-periodic case, we find that the algorithm is able to follow a branch of invariant tori even when the tori are resonant, provided that the encountered resonances are 'weak enough'; see §4.3 for details. Peaks in the estimated error, which is monitored during continuation, can actually be used to locate Arnol′d tongues. The algorithm works independently of the stability-type of the torus. It is able to 'step over' small parameter intervals where the torus changes stability during which process it loses normal hyperbolicity; see §5.2 for an example.

This paper is organised as follows. In §2 we give an overview of the historical background and a comparison of methods for the computation of invariant tori. Section §3 covers the derivation of an invariance equation for quasi-periodic invariant tori. Its discretisation by finite differences is described in detail in §4. In §5 we demonstrate the performance of our algorithm with examples. In particular, an example is given where a torus changes stability and a family of period-doubled tori emerges; see §5.2.

2. Historical Background. The first direct numerical approximations of invariant 2-tori appeared in the engineering literature about 20 years ago. Since quasi-periodic invariant 2-tori of dynamical systems can be observed directly as the closure of a quasi-periodic orbit, early attempts of the numerical investigation of quasi-periodic invariant 2-tori were based on the computation of quasi-periodic orbits. Chua and Ushida [15] described in 1981 the *spectral balance method* for the approximation of quasi-periodic orbits, which is a generalisation of the *harmonic balance method* used for the approximation of periodic orbits. A description of both methods can be found in [46]. The basic idea is to use Fourier polynomial approximations of the quasi-periodic orbit, where the set of basis functions must be chosen carefully to avoid small divisor problems. This method is suitable for the approximation of a single quasi-periodic orbit regardless of its stability. We use a slightly generalised version of this method in §5.2 for obtaining initial approximations to the 2-torus and its second basic frequency.

Another approach for the numerical analysis of quasi-periodic orbits was introduced by Kaas-Petersen [33, 34, 35] in 1985. Here, a quasi-periodic orbit is computed as a fixed point of a generalised Poincaré map. This algorithm is generalisable to quasi-periodic orbits on higher-dimensional tori and has the advantage that it provides a simple algebraic criterion for determining the stability of the orbit, which is directly related to the stability of the fixed point. Hence, it is straightforward to detect quasi-periodic bifurcations (see also [6] and [9]), and an example of a quasi-periodic orbit losing stability is given in [35]. The drawback of this algorithm is that it also suffers from the small divisor problem. Namely, for quasi-periodic orbits with rotation numbers that are well approximated by continued fraction expansion it becomes hard or even impossible to compute the generalised Poincaré map with sufficient precision.

To overcome difficulties caused by properties of the flow on the torus, such as the small divisor problem, research focused on the direct computation of the torus itself or, equivalently, an associated invariant closed curve of a local Poincaré map. In §2.1 we sketch the historical development and the current state of the art of methods for invariant closed curves and tori of maps, and in §2.2 we do the same for tori of ODEs. In the sequel, $\mathbb{T}^p := (\mathbb{R}/2\pi)^p$ denotes the p-dimensional standard torus parametrised over $[0, 2\pi)^p$. A function $u : \mathbb{T}^p \to \mathbb{R}$ with domain $\mathbb{T}^p$ is called *torus function*. Note

that $\mathbb{T}^1 = S^1$ and that by this definition the 0-torus $\mathbb{T}^0$ is a point, whereas the 0-sphere S^0 consists of two isolated points. For invariant 1-tori of maps and ODEs we also use the terms invariant closed curve and periodic orbit, respectively.

2.1. Tori of Maps. The basic idea is to find a torus function $u : \mathbb{T}^p \to \mathbb{R}^n$ such that its image $T := \{ u(\theta) \mid \theta \in \mathbb{T}^p \}$ is invariant under the map $f : \mathbb{R}^n \to \mathbb{R}^n$. That is, the invariance condition

$$u(\varphi(\theta)) = f(u(\theta)) \tag{2.1}$$

holds point-wise, where $\theta \in \mathbb{T}^p$ and $\varphi : \mathbb{T}^p \to \mathbb{T}^p$ is diffeomorphic to the map f restricted to the invariant torus T. Here, a typical problem that appears in torus computations becomes visible, namely, the invariance condition (2.1) provides only an equation for u, but the function φ is also unknown and it depends on the parametrisation of the torus T. One can fix the function φ by either introducing local coordinates or by adding further conditions to (2.1), a non-trivial task in both cases. Once the function φ is fixed, one transforms (2.1) into the equivalent fixed point form

$$u(\theta) = f(u(\varphi^{-1}(\theta))), \tag{2.2}$$

and solves (2.2), in principle, by fixed-point iteration or by applying Newton's method to one of the problems $u(\varphi(\theta)) - f(u(\theta)) = 0$ or $u(\theta) - f(u(\varphi^{-1}(\theta))) = 0$. We say 'in principle' because we have not specified conditions to fix φ, hence, (2.1) and (2.2) are not ready-to-use algorithms.

In 1985 Kevrekidis, Aris, Schmidt and Pelikan [36] published an algorithm for the computation of invariant closed curves based on the invariance condition (2.1) under the additional assumption that the map f is available in the so-called *partitioned form*, that is, it can be written as

$$f : \begin{pmatrix} r \\ \theta \end{pmatrix} \mapsto \begin{pmatrix} g(r,\theta) \\ h(r,\theta) \end{pmatrix},$$

where $\theta \in S^1$ and $r \in \mathbb{R}$. In other words, f is a map on the cylinder $S^1 \times \mathbb{R}$. Hence, the invariance condition becomes the functional equation $u(h(u(\theta),\theta)) = g(u(\theta),\theta)$ where only $u : S^1 \to \mathbb{R}$ is unknown and which can be solved efficiently with Newton's method. A generalisation of this algorithm to the case of invariant closed curves of general maps in $\mathbb{R}^n$ was proposed by Debraux [16] in 1994. Debraux adds suitable orthogonality conditions to fix the parametrisation. Another method was given in 1996 by Moore [41]. Here, a unique parametrisation is obtained by introducing a local coordinate system.

An algorithm for the computation of invariant closed curves of maps based on the fixed point equation (2.2) was published in 1987 by Van Veldhuizen [51, 52] where it is assumed that the invariant closed curve can be parametrised by radial coordinates. Thereby, the coordinate system is fixed and it is possible to compute attracting invariant closed curves by iterating the fixed-point equation (2.2). This algorithm can be regarded as a first implementation of the Hadamard graph transform technique; see also [31].

Dieci and Lorenz [19] proposed in 1995 a generalisation of the graph transform technique to the computation of attracting invariant tori of maps, and examples for 2-tori are given. With the aid of the normal bundle, a local torus-coordinate system is introduced to fix the parametrisation. Therefore, no restrictions on the representation of the map apply. This algorithm allows the computation of the full invariant 2-torus

of an ODE when applied to the time-τ map of the flow generated by the ODE. A recent implementation of a continuation method utilising this algorithm includes the re-parametrisation technique described in [41] and can be found in [48].

Independently, in 1996 Broer, Osinga and Vegter [10, 11, 12, 13] developed an algorithm for the computation of invariant tori of maps which is also based on the graph transform technique. This algorithm introduces a local coordinate system utilising the $\partial_x f$-invariant transversal bundle. It is able to compute attracting as well as saddle-type tori and examples of attracting and saddle-type invariant closed curves and 2-tori are given. Furthermore, their algorithm can be used for the computation of compact overflowing invariant manifolds, for instance, local stable and unstable manifolds of compact invariant manifolds. This is demonstrated with examples of the computation of local stable and unstable manifolds of invariant closed curves and invariant 2-tori; these examples appeared in [44].

A further developed version of this algorithm was published in 2003 by Broer, Hagen and Vegter [7]. Here, a Lipschitz-continuous approximation to the normal bundle is used instead of the $\partial_x f$-invariant transversal bundle. This algorithm is implemented on both fixed and adaptive meshes for invariant closed curves and 2-tori. Examples for the computation of attracting as well as saddle-type invariant closed curves and 2-tori of maps and ODEs are given.

2.2. Tori of ODEs. The second main class of algorithms for the computation of invariant tori of ODEs is based on the invariance condition for vector fields. The basic idea is to find a torus function $u : \mathbb{T}^p \to \mathbb{R}^n$ such that its image $T := \{\, u(\theta) \mid \theta \in \mathbb{T}^p \,\}$ is invariant under the flow induced by a vector field. In other words, the vector field restricted to the torus T is everywhere tangent to T. This invariance condition can be rewritten as the first-order partial differential equation (PDE)

$$\sum_{i=1}^{p} \psi_i(\theta) \frac{\partial u}{\partial \theta_i} = f(u)\,, \tag{2.3}$$

where the $\psi_i : \mathbb{T}^p \to \mathbb{R}$, $i = 1, \ldots, p$, are the coefficients of the vector field restricted to the invariant torus in the base $\{\frac{\partial u}{\partial \theta_1}, \ldots, \frac{\partial u}{\partial \theta_p}\}$. Again, one encounters the problem that (2.3) provides an equation for u only, while the function ψ is also unknown and depends on the choice of a parametrisation of the torus. As for the computation of invariant tori of maps, the function ψ can be fixed by either introducing local coordinates or by adding further conditions, either of which comes with its own difficulties. Once the function ψ is fixed, one applies Newton's method and obtains a fast-converging algorithm.

An early algorithm that follows this idea was published in 1987 by Samoilenko [49]. It is based on the invariance condition (2.3) under the additional assumption that the ODE is available in the partitioned form

$$\begin{cases} \dot{r} &= g(r, \theta), \\ \dot{\theta} &= h(r, \theta), \end{cases}$$

where $r \in \mathbb{R}^{n-p}$ and $\theta \in \mathbb{T}^p$. In other words, the ODE is already given in torus coordinates. In this case the invariance condition (2.3) assumes the specific form

$$\sum_{i=1}^{p} h_i(u, \theta) \frac{\partial u}{\partial \theta_i} = g(u, \theta)\,. \tag{2.4}$$

Samoilenko considers the computation of quasi-periodic invariant tori by the Fourier-Galerkin method applied to (2.4) and a thorough convergence analysis of this algorithm is given both in the linear and in the nonlinear case. (He also gives an introduction to the theory of quasi-periodic orbits; the derivation of our invariance equation in §3 is, in fact, based on properties of quasi-periodic orbits stated in [49].)

The numerical approximation of invariant tori independent of the flow on the torus was first considered by Dieci, Lorenz and Russell [17] in 1991. Equation (2.4) is discretised by a finite difference method and a proof of convergence is given in [18]. Other discretisation methods for equation (2.4) were also studied; see, for example, [4, 22, 25, 40]. The performance of these algorithms is demonstrated with examples for the computation of attracting invariant 2-tori.

An extension to the computation of invariant 2-tori of ODEs that cannot be transformed into radius-angle coordinates was published by Moore [41] in 1996. Moore introduces a local coordinate system around the torus and, thereby, fixes the unknown function ψ. He also addresses the problem that a suitable initial parametrisation may become inappropriate during a parameter continuation and develops a re-parametrisation technique which produces parametrisations of high quality. The other way to fix the function ψ, namely, the extension of equation (2.3) by suitable additional conditions, was recently proposed by Henderson (personnel communication 2003). This avoids the computation of local coordinates at the expense of adding orthogonality conditions for each mesh point. Within a parameter continuation this method would also require frequent re-parametrisations as done, for example, in [41].

2.3. Comparison. The two main approaches for the computation of invariant tori of maps and ODEs, namely, applying Newton's method to a functional equation and the graph transform technique, have inherent strengths and weaknesses. The functional equation approach has the advantage that one obtains quadratically convergent algorithms by employing Newton's method, whereas algorithms based on the graph transform technique are only linearly convergent. Furthermore, the speed of convergence of Newton's method is independent of the properties of the flow near the torus while the speed of convergence of the graph transform technique is determined by the attraction (expansion) transverse to the torus. In particular, during a parameter continuation, algorithms based on the graph transform technique cannot 'step over' small parameter intervals where the torus changes stability.

On the other hand, the graph transform technique is memory conservative. It requires only to store the mesh and can be implemented to work node by node. Thus, it is not necessary to have simultaneous access to the full stored data. In contrast, for applying Newton's method it is necessary to store not only the mesh but also a Jacobian and its (incomplete) factorisation. Therefore, compared with Newton's method, the graph transform technique allows the computation of higher dimensional tori under the restriction of sufficient normal attraction (expansion).

A complete proof of convergence for normally hyperbolic invariant tori is only available for algorithms based on the graph transform. Convergence of Newton's method was investigated seriously for algorithms using the invariance condition (2.4). The major difficulty here is to show stability of the discretisation. Such a proof of stability is given by Dieci and Lorenz [18] for a finite-difference scheme, but it requires rather strong assumptions.

A problem that both main approaches share is the choice of a suitable parametrisation, which is non-trivial as we already pointed out. This is the major difficulty for the construction of algorithms that are simple to implement. Our main goal is to

overcome this difficulty. As a first step we derive a PDE that gives rise to a parametrisation of quasi-periodic invariant tori in a natural way. The discretisation of this equation provides an algorithm that not only computes a quasi-periodic invariant torus but also its basic frequencies. The method is simple to implement, uses only information in the tangent space and can be regarded as a natural generalisation of algorithms for periodic orbits. Furthermore, it is used in a one-parameter continuation environment where it is capable of computing phase-locked tori, provided the resonances are 'sufficiently weak' relative to the used mesh; see §4.3.

3. Invariance Equation. In this section we derive an extended PDE that an invariant quasi-periodic torus must satisfy. To this end we make use of the close relationship between a quasi-periodic torus that is invariant under the flow of (1.1) and a quasi-periodic orbit that is an actual solution of (1.1). This is described in detail in Broer, Huitema and Sevryuk [8] and Samoilenko [49]. In the following we briefly quote the properties that we use for the derivation.

A quasi-periodic orbit of (1.1) densely fills a quasi-periodic invariant torus. Furthermore, any quasi-periodic orbit x can be written in the form $x(t) := u(\omega t)$, where $u : \mathbb{T}^p \to \mathbb{R}^n$ is a torus function and the real numbers $\omega_1, \ldots, \omega_p$ are *rationally independent*, that is, there exist no integers $k_1, \ldots, k_p$, $\sum_{i=1}^{p} |k_p| \neq 0$, such that $\sum_{i=1}^{p} k_i \omega_i = 0$. The numbers $\omega_1, \ldots, \omega_p$ are called the *basic frequencies* and $\omega := (\omega_1, \ldots, \omega_p)$ the *frequency basis* of a quasi-periodic torus or a quasi-periodic orbit, respectively.

An important property that we are going to use is the following equality of norms. In the space of quasi-periodic functions $x \in [\, \mathcal{C}^0(\mathbb{R}) \,]^n$ we define the supremum norm

$$\|x\|^2_{[\, \mathcal{C}^0(\mathbb{R}) \,]^n} := \sum_{i=1}^{n} \left(\sup_{t \in \mathbb{R}} |x_i(t)| \right)^2 ,$$

and in the space of torus functions the maximum norm

$$\|u\|^2_{[\, \mathcal{C}^0(\mathbb{T}^p) \,]^n} := \sum_{i=1}^{n} \left(\max_{\theta \in \mathbb{T}^p} |u_i(\theta)| \right)^2 .$$

If x is a quasi-periodic orbit with frequency basis ω and u an associated torus function such that $x(t) := u(\omega t)$ then the norms of x and u have the same value (see also [49]) :

$$\|x\|_{[\, \mathcal{C}^0(\mathbb{R}) \,]^n} = \|u\|_{[\, \mathcal{C}^0(\mathbb{T}^p) \,]^n} , \tag{3.1}$$

which follows from the density property mentioned above.

Now, let $y \in [\mathcal{C}^1(\mathbb{R})]^n$ be an arbitrary quasi-periodic function with frequency basis ω and let $v \in [\, \mathcal{C}^1(\mathbb{T}^p) \,]^n$ be an associated torus function. We put the representation $y(t) = v(\omega t)$ into (1.1) and define the quasi-periodic function $g \in [\, \mathcal{C}^0(\mathbb{R}) \,]^n$,

$$g(t) := f(v(\omega t)) - \sum_{i=1}^{p} \omega_i \frac{\partial v}{\partial \theta_i}(\omega t) ,$$

and the associated torus function $G \in [\, \mathcal{C}^0(\mathbb{T}^p) \,]^n$,

$$G(\theta) := f(v(\theta)) - \sum_{i=1}^{p} \omega_i \frac{\partial v}{\partial \theta_i}(\theta) .$$

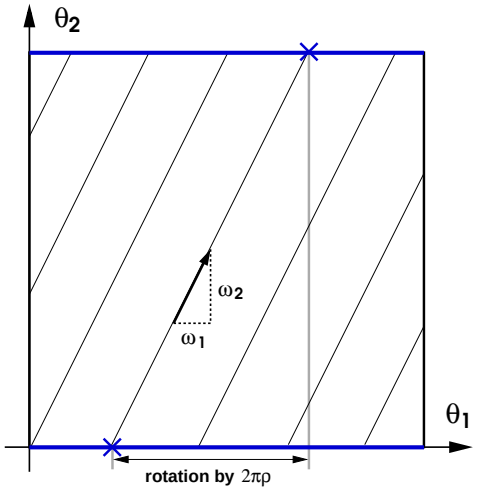

FIGURE 3.1. *The characteristic field of equation (3.2) on the standard torus $\mathbb{T}^2$ is a set of parallel straight lines with slope $\varrho = \omega_2/\omega_1$. The cross-section $\theta_2 = 0$ (blue lines) is mapped onto itself under the transport along the characteristics whereby a rotation by $2\pi/\varrho$ occurs.*

We can interpret the function g as a defect function. If y is a quasi-periodic orbit of (1.1) then g is identically zero and vice versa. From the norm equality (3.1) of g and G we now obtain the equivalence

$$g \equiv 0 \quad \Longleftrightarrow \quad G \equiv 0\,,$$

which implies that a quasi-periodic torus u with frequency basis ω is invariant under the flow of (1.1) if and only if it satisfies the partial differential equation

$$\sum_{i=1}^{p} \omega_i \frac{\partial u}{\partial \theta_i} = f(u)\,. \tag{3.2}$$

Equation (3.2) has some remarkable properties that are closely related to the properties of the flow on the torus. Its characteristics satisfy the simple ordinary differential equation

$$\dot{\theta} = \omega\,, \qquad \theta \in \mathbb{T}^p\,,$$

which is solved by a set of parallel straight lines; see Fig. 3.1. In the following we denote a solution of (3.2) by u^*. The image $x(t) := u^*(\omega t)$ of a characteristic under the solution u^* in the phase-space of (1.1) is, by definition, a quasi-periodic orbit on the invariant torus T. Therefore, u^* maps the parallel flow generated by the characteristic equation on $\mathbb{T}^p$ onto the quasi-periodic flow on the invariant torus T. For that reason, we call a parametrisation of T generated by a solution of equation (3.2) a *natural parametrisation* of the torus T.

Since equation (3.2) is a semi-linear transport equation, arbitrary subsets $M \subseteq \mathbb{T}^p$ are transported along the characteristics without changing shape; see [23]. Of special interest are the cross-sections

$$T_i := \{\, \theta \in \mathbb{T}^p \mid \theta_i = 0 \,\}\,;$$

see Fig. 3.1, where T_2 is indicated by blue lines. After the time $t_i := 2\pi/\omega_i$ the set T_i is mapped onto itself whereby in each angular direction a shift of $2\pi\sigma_j$ occurs, where $\sigma_j = \omega_j/\omega_i$ and $j \neq i$. For $p = 2$ this is a rigid rotation with irrational rotation number. Therefore, each image set $u^*(T_i)$ is an invariant $(p-1)$-torus of the period-$2\pi/\omega_i$ stroboscopic map $P_i : u^*(T_i) \mapsto u^*(T_i)$.

A further noteworthy property of equation (3.2) is that it can be interpreted as a direct generalisation of the equations for equilibrium points (0-tori) and periodic orbits (1-tori) of autonomous differential equations, namely

$$0 = f(u)$$

and

$$\omega \frac{du}{dt} = f(u),$$

respectively. The latter is usually transformed such that the period of the periodic orbit rather than its frequency appears as a variable; see also [20].

Similar to periodic orbits, an invariant quasi-periodic torus of (1.1) is not uniquely defined by the partial differential equation (3.2). For any quasi-periodic invariant p-torus, both the torus function u and the frequency basis ω are unknown but (3.2) is an equation for the torus function only. This is due to the fact that the p-torus T has p *free phases*. In order to fix the free phases and allow the computation of the basis frequencies we introduce *phase conditions* as follows.

Assume that we already know a nearby solution $\tilde{u}$, for instance from a previous continuation step. Then we take $s \in \mathbb{T}^p$ such that the parametrisation $u(\theta + s)$ is an extremal point of the function

$$g(s) := \|\tilde{u} - u\|^2 ,$$

where we use the $[\,\mathcal{L}_2(\mathbb{T}^p)\,]^n$-norm defined by

$$\|u\|^2 := \frac{1}{(2\pi)^p} \sum_{i=1}^{n} \int_{\mathbb{T}^p} u(\theta)^2 \, d\theta \,.$$

This idea generalises the phase condition used in AUTO [20] and in [21] for the computation of periodic orbits. The parametrisation $u^*(\theta) := u(\theta + s^*)$ is implicitly defined by the necessary conditions of extremality of $g(s^*)$,

$$\left\langle \frac{\partial \tilde{u}}{\partial \theta_i} \,,\, u \right\rangle := \frac{1}{(2\pi)^p} \sum_{j=1}^{n} \int_{\mathbb{T}^p} \frac{\partial \tilde{u}_j}{\partial \theta_i}(\theta)\, u_j(\theta)\, d\theta = 0 \,, \qquad i = 1, \ldots, p \,.$$

By adding these phase conditions to equation (3.2) we obtain the extended system

$$\left\{ \begin{array}{rcl} \displaystyle\sum_{i=1}^{p} \omega_i \frac{\partial u}{\partial \theta_i} & = & f(u) \,, \\ \\ \left\langle \dfrac{\partial \tilde{u}}{\partial \theta_i} \,,\, u \right\rangle & = & 0 \,, \qquad i = 1, \ldots, p \,, \end{array} \right. \tag{3.3}$$

which has as many equations as unknowns and where $\tilde{u}$ is an a-priori known initial approximation. We refer to system (3.3) as the *invariance equation*.

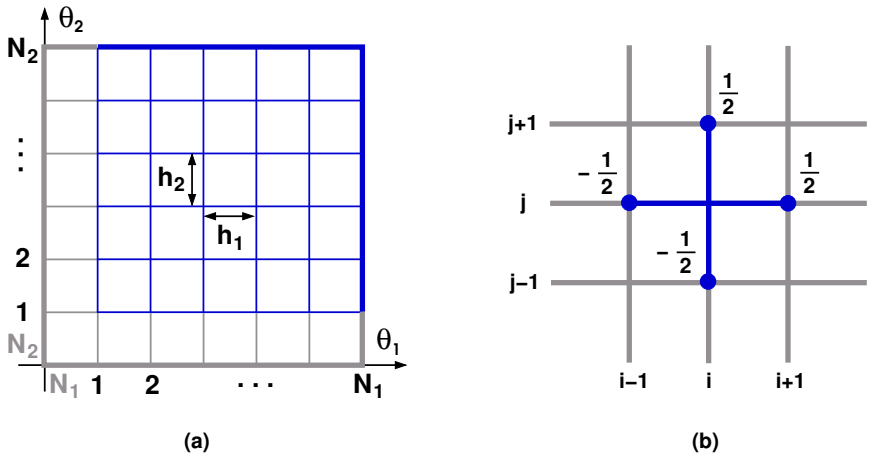

FIGURE 4.1. *Discretisation of the two-dimensional standard torus* $\mathbb{T}^2$ *(a); the periodicity with respect to* θ_1 *and* θ_2 *is indicated by grey colouring; only the data of the blue part of the mesh needs to be stored. The finite-difference star generated by the common central finite-difference quotient is shown in panel (b).*

4. Numerical Approximation. In this section we describe the computation of approximate solutions of the invariance equation (3.3). To this end, we introduce appropriate mesh-functions and approximate the partial derivatives by central difference quotients; see §4.1. Because of the specific structure of the invariance equation (3.3) the discretised system can be constructed recursively, whereby the dimension p of the torus is used as the recursion parameter; see §4.4. This already reduces the implementation effort in the case of 2-tori and means that our implementation of the proposed algorithm is able to compute invariant tori of arbitrary fixed dimension p. In §4.2 we discuss convergence of the algorithm and in §4.3 we explain how to integrate it in a continuation environment. In §4.3 we also address existence and convergence problems that may occur since quasi-periodic invariant tori do not persist under generic perturbations.

4.1. Discretisation by Finite Differences. A discretisation of equation (3.3) by finite differences seems especially advantageous for the following reasons:

1. The domain $\mathbb{T}^2$ is compact and has no boundary.
2. High-order finite-difference schemes are easy to construct.
3. The finite-difference method is simple to implement.

In order to construct a mesh, we choose p arbitrary but fixed natural numbers $N_1, \ldots, N_p$ and call $N := \min\{N_1, \ldots, N_p\}$ the *discretisation parameter*. We define the *step-sizes* $h_i := 2\pi/N_i$, $i = 1, \ldots, p$, and call $h := \max\{h_1, \ldots, h_p\} = 2\pi/N$ the *mesh size*. The mesh points are now defined using the one-dimensional toroidal index-sets $\mathbb{T}_{N_i} := \mathbb{Z}/N_i$, $i = 1, \ldots, p$, and

$$\mathbb{T}_N^p := (\mathbb{T}_{N_1}) \times \cdots \times (\mathbb{T}_{N_p})$$

is the corresponding p-dimensional toroidal multi-index set; see Fig. 4.1 (a). The mesh-functions are defined on the space $\mathbb{G}_N$:

$$\mathbb{G}_N := \{\, u_N \mid u_N : \mathbb{T}_N^p \to \mathbb{R} \,\}\,.$$

m	η_k				q	
1	$\frac{1}{2}$				2	$x \in \mathcal{C}^3(\mathbb{R})$
2	$\frac{8}{12}$	$-\frac{1}{12}$			4	$x \in \mathcal{C}^5(\mathbb{R})$
3	$\frac{45}{60}$	$-\frac{9}{60}$	$\frac{1}{60}$		6	$x \in \mathcal{C}^7(\mathbb{R})$
4	$\frac{672}{840}$	$-\frac{168}{840}$	$\frac{32}{840}$	$-\frac{3}{840}$	8	$x \in \mathcal{C}^9(\mathbb{R})$

TABLE 4.1

Coefficients for several central finite-difference schemes. These schemes are consistent and of order q for sufficiently smooth functions, as specified in the last column

A mesh-function on $\mathbb{T}_N^p$ is indicated by the sub-index N. Addition of two mesh-functions and multiplication with a scalar are defined point-wise. In the space of vector-valued mesh functions $[\,\mathbb{G}_N\,]^n$ we define a scalar product as

$$\langle\, u_N\,,\, v_N\,\rangle_{[\,\mathbb{G}_N\,]^n} := \sum_{i=1}^{n} \langle\, u_{N,i}\,,\, v_{N,i}\,\rangle_{\mathbb{G}_N}\,,$$

where we used the scalar product in the space of real-valued mesh functions $\mathbb{G}_N$ on the right-hand side:

$$\langle\, u_{N,i}\,,\, v_{N,i}\,\rangle_{\mathbb{G}_N} := \frac{1}{N_1 \cdots N_p} \sum_{j \in \mathbb{T}_N^p} u_{N,i}(j) v_{N,i}(j)\,.$$

In the space $[\,\mathbb{G}_N\,]^n$ we use the norm which is induced by the scalar product

$$\|u_N\|^2_{[\,\mathbb{G}_N\,]^n} := \langle\, u_N\,,\, u_N\,\rangle^2_{[\,\mathbb{G}_N\,]^n}\,.$$

We now discretise the invariance equation (3.3) by restricting to functions defined only on the mesh points $\mathbb{T}_N^p$. We denote this discretisation in terms of the discretisation operator $P_N : [\,\mathcal{C}^r(\mathbb{T}^p)\,]^n \to [\,\mathbb{G}_N\,]^n$, sometimes also referred to as the restriction operator,

$$(P_N u)(j_1, \ldots, j_p) := u(j_1 h_1, \ldots, j_p h_p)\,. \tag{4.1}$$

Furthermore, we approximate the partial differential operators by the partial finite-difference operators $\partial_{N,i} : [\,\mathbb{G}_N\,]^n \to [\,\mathbb{G}_N\,]^n$,

$$\partial_{N,i} u_n := \frac{1}{h_i} \sum_{k=-m}^{m} \eta_k u_N(\ldots, j_i + k, \ldots)\,, \qquad \eta_k \in \mathbb{R}\,,\ \ i = 1, \ldots, p\,,$$

where we use central finite-difference quotients for which the coefficients η_k are skew symmetric, that is, $\eta_k = -\eta_{-k}$ for $k = 0, \ldots, m$.

For different values of m the coefficients η_k, $k = 1, \ldots, m$, of consistent central difference schemes are given in Table 4.1; see also [30]. Note that $\eta_0 = 0$ by skew symmetry. For $m = 1$ this is the common 3-point central-difference quotient formula $\dot{x}(t) = \frac{1}{2h}(x(t+h) - x(t-h)) + \mathcal{O}(h^2)$ of order 2 and its difference star is shown in Fig. 4.1 (b). In our implementation we use the two finite-difference discretisations for $m = 1$ and $m = 2$ of consistency order 2 and 4, respectively, and compute two different approximations on the same mesh. This allows us to estimate the approximation error as the norm of the difference between these two solutions.

We introduce a compact notation for this discretisation by using the difference operator $D_N : [\,\mathbb{G}_N\,]^n \to [\,\mathbb{G}_N\,]^n$,

$$D_N u_n := \sum_{i=1}^{p} \omega_i \partial_{N,i} u_N, \tag{4.2}$$

and define for brevity

$$f_N(u_N)(j_1,\ldots,j_p) \;:=\; P_N(\,f(u(\theta))\,)(j_1,\ldots,j_p) \;=\; f(u(j_1h_1,\ldots,j_ph_p))\,.$$

With these definitions the discretised invariance equation (3.3) is given by

$$\left\{ \begin{array}{rcll} D_N u_N & = & f_N(u_N)\,, & \\ \langle\, \partial_{N,i} P_N \tilde{u}\,,\, u_N \,\rangle & = & 0\,, & i = 1,\ldots,p\,. \end{array} \right. \tag{4.3}$$

In practical implementations it is recommended to use normalised difference quotients for $\partial_{N,i} P_N \tilde{u}$ because this usually leads to better conditioned systems.

System (4.3) can be solved by applying Newton's method. Therefore, it is convenient to rewrite (4.3) as the root-finding problem

$$F_N(u_N,\omega) := \left(\begin{array}{c} f_N(u_N) - D_N u_N \\ \langle\, \partial_{N,i} P_N \tilde{u}\,,\, u_N \,\rangle \end{array} \right) = 0\,, \tag{4.4}$$

where $F_N : ([\,\mathbb{G}_N\,]^n \times \mathbb{R}^p) \to ([\,\mathbb{G}_N\,]^n \times \mathbb{R}^p)$. Note that the dependence of F_N on ω is due to the dependence of D_N on ω which, for simplicity, is not explicitly noted.

4.2. Consistency and Stability. So far, we only assumed for the construction of our algorithm that a sufficiently smooth solution of the invariance equation (3.3) exists in order for the difference-quotients to be meaningful. Although, in addition, we generally need regularity of the solution for applying Newton's method (which follows from normal hyperbolicity), a rigorous proof of convergence can only be given in a rather restrictive setting. The restrictions are caused by properties of the right-hand side f of the autonomous system (1.1) that we have to impose in order to show stability of the finite-difference discretisation. These properties are similar to properties required in the proofs of convergence given by Dieci, Lorenz and Russell [17] and by Dieci and Lorenz [18] for finite difference methods and by Samoilenko [49] for Galerkin methods, as outlined below.

The proof of stability of our finite-difference discretisation in the case when one or more basic frequencies are unknown is ongoing work and we restrict here to the special case when quasi-periodic forcing is present and focus on similarities to and differences with [17], [18] and [49]. To set the stage, we consider the ODE in partitioned form

$$\left\{ \begin{array}{rcll} \dot{x} & = & f(x,\theta)\,, & f : \mathbb{R}^n \times \mathbb{T}^p \to \mathbb{R}^n\,, \quad n \geq 1\,, \\ \dot{\theta} & = & \omega\,, & \omega \in \mathbb{R}^p\,, \end{array} \right. \tag{4.5}$$

where ω is now a known quantity. Since f now explicitly depends on θ, an invariant torus of (4.5) has no free phases and the invariance equation (3.3) reduces to the partial differential equation

$$\sum_{i=1}^{p} \omega_i \frac{\partial u}{\partial \theta_i} = f(u,\theta) \tag{4.6}$$

with constant coefficients $\omega_1, \ldots, \omega_p$. In other words, the invariance equation is no longer extended. Equation (4.6) is a special case of the partial differential equation (2.4), which is used as the determining equation for invariant tori in [17], [18] and [49]. As before we denote a solution of equation (4.6) by u^*.

To simplify the following considerations we define the differential operator $D : [\,\mathcal{C}^r(\mathbb{T}^p)\,]^n \to [\,\mathcal{C}^{r-1}(\mathbb{T}^p)\,]^n$ as $D := \sum_{i=1}^p \omega_i \frac{\partial}{\partial \theta_i}$. With this definition we can rewrite the continuous and the discretised problems as

$$Du = f(u, \theta) \tag{4.7}$$

and

$$D_N u_N = f_N(u_N)\,, \tag{4.8}$$

respectively. Equation (4.8) is consistent of order q with equation (4.7) at u^* if there exist constants $M_1, M_2 \in \mathbb{R}$ independent of N and a natural number N_0 such that for all $N \geq N_0$ the inequalities

$$\|P_N D u^* - D_N P_N u^*\| \leq M_1 h^q$$

and

$$\|P_N f(u^*, \theta) - f_N(P_N u^*)\| \leq M_2 h^q$$

hold. The second inequality holds trivially because $P_N f(u^*, \theta) - f_N(P_N u^*) = 0$ by definition of P_N. We can construct high-order finite-difference schemes by using one-dimensional standard difference-quotient formulas as stated in the following lemma. Note that, in contrast to [17] and [18], we do not use upwind schemes.

LEMMA 4.1 (consistency). *Let $x \in \mathcal{C}^r(\mathbb{R})$ and the difference quotient, defined as*

$$\Delta x(t) := \frac{1}{h} \sum_{k=1}^{m} \eta_k (x(t + kh) - x(t - kh))\,,$$

be consistent with order q (see Table 4.1), that is, there exist continuous functions $h_0(t) > 0$ and $0 \leq C(t) < \infty$ such that for every $t \in \mathbb{R}$ and $h \in [0, h_0(t))$ the inequality

$$\left| \frac{dx}{dt}(t) - \Delta x(t) \right| \leq C(t) h^q$$

holds. Then for $u^* \in [\,\mathcal{C}^r(\mathbb{T}^p)\,]^n$ there exists a natural number N_0 such that the finite-difference operator D_N is consistent of order q with D at u^* for all $N \geq N_0$.

Note that $x \in \mathcal{C}^{q+1}(\mathbb{R})$ is a sufficient condition for the construction of consistent difference quotients of order q. Then $C(t) = \|x\|_{\mathcal{C}^{q+1}(\mathbb{R})}$ and the inequality in the lemma holds for arbitrary $h > 0$. The condition $x \in \mathcal{C}^{q+1}(\mathbb{R})$ can be weakened; see [28].

Proof. First we show consistency of the partial finite difference operator from which the assertion then follows.

For $u \in \mathcal{C}^r(\mathbb{T}^p)$ we denote by $\partial_i u(\theta) := \Delta u(\cdots, \theta_i, \cdots)$ the partial differential quotient defined by applying Δ to the i-th argument of u. Then, by assumption, there exist continuous functions $h_{ij}(\theta) > 0$ and $0 \leq C_{ij}(\theta) < \infty$ such that for each component u_j^*, $j = 1, \ldots, n$, and every $\theta \in \mathbb{T}^p$ the inequality $|\frac{\partial}{\partial \theta_i} u_j^*(\theta) - \partial_i u_j^*(\theta)| \leq C_{ij}(\theta) h^q$

holds for all $h \in [0, h_{ij}(\theta))$. From compactness of $K := \{1,\dots,p\} \times \{1,\dots,n\} \times \mathbb{T}^p$ it follows that both $h_0 := \min_{(i,j,\theta)\in K} h_{ij}(\theta) > 0$ and $C_0 := \max_{(i,j,\theta)\in K} C_{ij}(\theta) < \infty$ exist. Therefore, the inequality $|\frac{\partial}{\partial\theta_i} u_j^*(\theta) - \partial_i u_j^*(\theta)| \le C_0 h^q$ holds uniformly for all $\theta \in \mathbb{T}^p$ and $h \in [0, h_0)$. From $(\partial_{N,i} P_N u_j^*)(k_1,\dots,k_p) = \partial_i u_j^*(k_1 h_1,\dots,k_p h_p)$ follows now the estimate

$$\left\| P_N \frac{\partial u^*}{\partial \theta_i} - \partial_{N,i} P_N u^* \right\|^2 = \sum_{j=1}^{n} \left\| P_N \left(\frac{\partial u_j^*}{\partial \theta_i} - \partial_i u_j^* \right) \right\|^2 \le \sum_{j=1}^{n} (C_0 h^q)^2 = n (C_0 h^q)^2 \,,$$

where the '$\le$' sign is obtained using the triangle inequality. This implies consistency of $\partial_{N,i}$ for $i = 1,\dots,p$.

Let now $\tau_i := P_N \frac{\partial}{\partial\theta_i} u^* - \partial_{N,i} P_N u^*$, then $P_N D u^* - D_N P_N u^* = \sum_{i=1}^{p} \omega_i \tau_i$ and we obtain the estimate

$$\|P_N D u^* - D_N P_N u^*\|^2 = \left\| \sum_{i=1}^{p} \omega_i \tau_i \right\|^2 \le \left\| \sum_{i=1}^{p} \omega_i \|\tau_i\| \right\|^2 \le \left| \sum_{i=1}^{p} \omega_i \right|^2 n (C_0 h^q)^2 \,,$$

and thus the assertion with $N_0 > 1/h_0$. □

To simplify the notation of stability we define the linear operators A_N and L_N as follows. Let $J(\theta)$ denote the Jacobian $\frac{\partial}{\partial x} f(u^*(\theta), \theta)$ at $(u^*(\theta), \theta)$. Then we define the discrete linear operator $A_N : \mathbb{G}_N \to \mathbb{G}_N$ point-wise as

$$(A_N u_N)(j_1,\dots,j_p) := J(j_1 h_1,\dots,j_p h_p)\, u_N(j_1,\dots,j_p) \,,$$

and $L_N : \mathbb{G}_N \to \mathbb{G}_N$ becomes $L_N := A_N - D_N$. Note that, similar to (4.4) for our specific invariance equation (4.6), L_N is the Jacobian $F_N'(P_N u^*)$ of F_N evaluated at $P_N u^*$.

Our finite-difference discretisation is stable if for some $N_0 \in \mathbb{N}$ the inverse operators L_N^{-1} exist and are uniformly bounded for all $N \ge N_0$. In order to show stability we impose a further restriction on f as stated now.

LEMMA 4.2 (stability). *Suppose the Jacobian $J(\theta)$ is uniformly strongly positive, that is, there exists a constant $c > 0$ independent of θ such that the inequality $\langle\, J(\theta)x \,,\, x \,\rangle \ge c\|x\|^2$ holds for all $x \in \mathbb{R}^n$. Then the finite-difference discretisation for equation (4.6) defined by (4.8) is stable. More precisely, the inverse operators L_N^{-1} exist for $N \ge N_0 \ge 2m+1$ and are uniformly bounded by $\|L_N^{-1}\| \le c^{-1}$.*

Proof. We divide the proof into two parts. First, we show that the discretisation is stable, provided D_N is skew-symmetric. Second, we show that D_N is skew-symmetric for our choice of discretisation.

Suppose D_N is skew-symmetric for all $N \ge N_0 \in \mathbb{N}$, that is, $D_N^* = -D_N$. Then $\langle\, D_N u_N \,,\, u_N \,\rangle = \langle\, u_N \,,\, -D_N u_N \,\rangle = -\langle\, D_N u_N \,,\, u_N \,\rangle = 0$. It follows for L_N the equality

$$\langle\, L_N u_N \,,\, u_N \,\rangle = \langle\, (A_N - D_N) u_N \,,\, u_N \,\rangle = \langle\, A_N u_N \,,\, u_N \,\rangle \,. \tag{4.9}$$

From the definition of the scalar product in $\mathbb{G}_N$ and the assumption on $J(\theta)$ we obtain the inequality

$$\begin{aligned} \langle\, A_N u_N \,,\, u_N \,\rangle &= \frac{1}{N_1 \cdots N_p} \sum_{j \in \mathbb{T}_N^p} \langle\, (A_N u_N)(j) \,,\, u_N(j) \,\rangle_{\mathbb{R}^n} \\ &\ge \frac{1}{N_1 \cdots N_p} \sum_{j \in \mathbb{T}_N^p} c \langle\, u_N(j) \,,\, u_N(j) \,\rangle_{\mathbb{R}^n} \\ &= c\|u_N\|^2. \end{aligned}$$

This implies stability: $c\|u_N\|^2 \le \langle\, L_N u_N \,,\, u_N \,\rangle \le \|L_N u_N\|\|u_N\|$. Thus, $c\|u_N\| \le \|L_N u_N\|$ for all $u_N \in \mathbb{G}_N$, hence, the inverse operators L_N^{-1} exist and are uniformly bounded by $\|L_N^{-1}\| \le c^{-1}$.

In order to show skew-symmetry of D_N we introduce the rotation operators $E_i : \mathbb{G}_N \to \mathbb{G}_N$, $(E_i u_N)(j_1,\ldots,j_i,\ldots,j_p) := u_N(j_1,\ldots,j_i+1,\ldots,j_p)$. Using E_i, the partial difference operators can be written as $\partial_{N,i} = (1/h_i)\sum_{k=1}^m \eta_k(E_i^k - E_i^{-k})$, the assumption $N_0 \ge 2m+1$ eliminates the pathological case that $E_i^k = E_i$ for some $k = 2,\ldots,m$. In the next step we confirm that $E_i^* = E_i^{-1}$. By definition, we have

$$\langle\, E_i u_N \,,\, v_N \,\rangle = \frac{1}{N_1 \cdots N_p} \sum_{j \in \mathbb{T}_N^p} \langle\, u_N(\cdots, j_i+1, \cdots) \,,\, v_N(\cdots, j_i, \cdots) \,\rangle.$$

The index shift $(j_1,\ldots,j_i+1,\ldots,j_p) \mapsto (\tilde{\jmath}_1,\ldots,\tilde{\jmath}_i,\ldots,\tilde{\jmath}_p)$ gives

$$\begin{aligned}\langle\, E_i u_N \,,\, v_N \,\rangle &= \frac{1}{N_1 \cdots N_p} \sum_{\tilde{\jmath} \in \mathbb{T}_N^p} \langle\, u_N(\cdots, \tilde{\jmath}_i, \cdots) \,,\, v_N(\cdots, \tilde{\jmath}_i - 1, \cdots) \,\rangle \\ &= \langle\, u_N \,,\, E_i^{-1} v_N \,\rangle\,,\end{aligned}$$

because we can reorder the sum over $\tilde{\jmath}_i$ due to the congruence $1 \cong N_i + 1 \pmod{N_i}$.

It follows that

$$\begin{aligned}(\partial_{N,i})^* &= \left(\frac{1}{h_i}\sum_{k=1}^m \eta_k(E_i^k - E_i^{-k})\right)^* &&= \frac{1}{h_i}\sum_{k=1}^m \eta_k\left((E_i^k)^* - \left((E_i^*)^k\right)^*\right) \\ &= \frac{1}{h_i}\sum_{k=1}^m \eta_k\left((E_i^*)^k - ((E_i^*)^*)^k\right) &&= \frac{1}{h_i}\sum_{k=1}^m \eta_k\left((E_i^{-1})^k - E_i^k\right) \\ &= -\frac{1}{h_i}\sum_{k=1}^m \eta_k\left(E_i^k - E_i^{-k}\right) &&= -\partial_{N,i}\,,\end{aligned}$$

thus

$$(D_N)^* = \left(-\sum_{i=1}^p \omega_i\, \partial_{N,i}\right)^* = -\sum_{i=1}^p \omega_i\, (\partial_{N,i})^* = \sum_{i=1}^p \omega_i\, \partial_{N,i} = -D_N,$$

which completes the proof. □

The condition that J be uniformly strongly positive can be interpreted geometrically. Writing $S(\theta) := \frac{1}{2}(J(\theta)+J(\theta)^{\mathrm{T}})$ and $U(\theta) := \frac{1}{2}(J(\theta)-J(\theta)^{\mathrm{T}})$ for the symmetrical and skew-symmetrical parts of $J(\theta)$, respectively, it follows from (4.9) that the uniform strong positivity of J is equivalent to S being uniformly positive definite. Hence, all eigenvalues of $S(\theta)$ are real and bounded from below by c. This implies that the eigenvalues of $J(\theta)$ have positive real parts that are also bounded from below by c, which means that the torus is normally repelling with a rate not less than $c > 0$. A similar argument leads to the torus being normally attracting by reversing time. However, as already stated at the beginning of this section, we conjecture that the only property of the solution required for convergence is its normal hyperbolicity. We show with our examples in §5 that our algorithm is indeed able to compute tori of saddle type.

We point out that we impose exactly the same condition on the Jacobian J as Dieci and Lorenz in [18]. However, the proof of stability given in [18] does not apply in our situation because L_N is not a block M-matrix, which is due to the fact that D_N is skew symmetric. On the other hand, this condition on J is weaker than the conditions used by Samoilenko in [49] to show convergence of the Galerkin method in the space $[\,\mathcal{C}^r(\mathbb{T}^p)\,]^n$. In [49] further constraints are required involving higher derivatives of f.

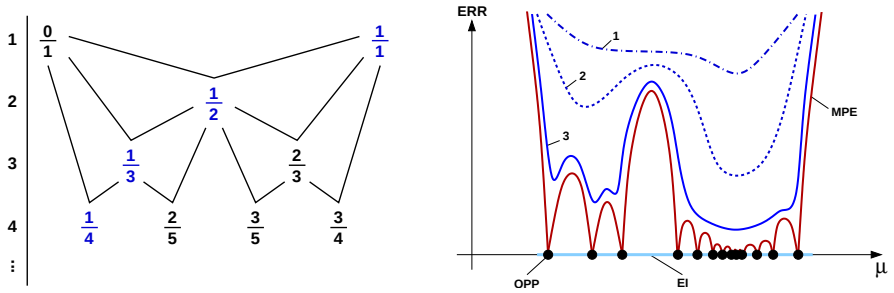

(a) (b)

FIGURE 4.2. *The first steps in the computation of the Farey tree* (*a*) *and a sketch of the expected convergence behaviour of our algorithm during a parameter continuation* (*b*). *For increasing but fixed discretisation parameter N we expect the estimated error ERR that depends on the parameter* μ *to behave qualitatively similar to the blue lines in the sequence 1-2-3. The points QPP on the* μ*-axis mark the parameter values where the torus is quasi-periodic. The light blue line segment EI indicates the open interval for which a solution of the discretised system exists. The maximal possible accuracy of our algorithm is drawn as the red curve MPE, the estimated error is bounded from below by* $\mathrm{ERR} \geq MPE$.

4.3. Continuation. A typical continuation algorithm consists of two parts, a predictor and a corrector. Suppose we already know a quasi-periodic invariant torus for a certain parameter value. Then the continuation algorithm proceeds as follows. First, the predictor computes an initial guess of a torus for a new parameter value. For example, this could be the known torus for the other parameter value or a torus obtained by extrapolation which is the basic idea of the tangent predictor. In the second step, the corrector computes the new quasi-periodic invariant torus starting from the initial guess produced by the predictor. Within this context our algorithm is a corrector.

During a parameter continuation the parameter will frequently cross Arnol′d tongues as we already pointed out in §1. Therefore, the invariance equation (3.3) does not hold on an open and dense set of parameter values. On the other hand, since our algorithm is stable, a solution of the discretised invariance equation (4.3) is regular, hence, it does exist not only for parameter values μ where the torus is quasi-periodic but also in a small neighbourhood of μ. Furthermore, any actual discretisation is of finite accuracy only. Therefore, we can expect that the algorithm also computes approximations to phase-locked tori, provided the resonance is 'weak enough'.

The terms *weaker resonance*, *stronger resonance* and *weak enough resonance* are used in the following sense. Utilising the Farey sum, one can introduce an ordering of resonances; see, for example, [26]. Let $\varrho_1 := p_1/q_1$ and $\varrho_2 := p_2/q_2$ be rational numbers. The *Farey sum* $\oplus$ is defined by $\varrho_1 \oplus \varrho_2 := (p_1 + p_2)/(q_1 + q_2)$. Starting with the rational numbers $\varrho_0 = 0/1$ and $\varrho_1 = 1/1$ one can introduce an ordering of p:q resonances with rational rotation number $\varrho \in (0, 1]$, $\varrho := p/q$, in terms of levels in the Farey tree; see Fig. 4.2 (a). For a given level, all rational rotation numbers above this level have smaller denominators. Similarly, all rational rotation numbers in lower levels have larger denominators. Because the width of an Arnol′d tongue that belongs to the rotation number p/q is proportional to ε^q (see Fig. 1.1 and [26]), all rotation numbers in higher levels belong to wider Arnol′d tongues and all rotation numbers in lower levels belong to more narrow Arnol′d tongues, thus, to stronger or weaker resonances, respectively. In particular, the Arnol′d tongue of $\varrho_1 \oplus \varrho_2$ is the widest Arnol′d tongue between the tongues of ϱ_1 and ϱ_2. The rotation numbers 1/1, 1/2, 1/3

and 1/4 play a special role and are called *strong resonances*; see, for example, [27]. If a rotation number belongs to a level such that for a given ODE the flow on the torus can be regarded as quasi-periodic within the accuracy of a particular discretisation, we call the resonance weak enough.

Within a continuation method we expect our algorithm to behave qualitatively as depicted in Fig. 4.2 (b). Suppose that the flow on the torus is quasi-periodic for the parameter values μ marked by the points QPP and that the solution of the discretised system exists for all parameter values in the interval marked by EI (entire light blue segment). Then the red curve MPE sketches the maximal possible accuracy that our algorithm can reach theoretically when the flow on the torus is not quasi-periodic. The blue lines with labels 1, 2 and 3 illustrate the actual accuracy for discretisations with discretisation parameters $0 < N_1 < N_2 < N_3$, respectively. An estimate of this accuracy must be monitored during continuation.

As long as the encountered resonances are weak enough, our algorithm will compute a solution within its prespecified numerical accuracy. For μ-values that belong to stronger resonances the actual accuracy of the obtained mesh function will not improve as the mesh is refined. Thus, we expect peaks in the approximation error due to wider Arnol′d tongues, the height of which indicates the 'strength' of a resonance. For all other parameter values we expect to observe convergence. When the parameter value gets close to a region where the torus is strongly resonant, the algorithm will eventually break down. Our experience is that the algorithm is less sensitive for finer meshes in the sense that the computed solutions seem smoother and we can continue closer to or even through strong resonances. Furthermore, for finer meshes the continuation routine requires fewer steps to pass through a stronger resonance tongue. After passing through an Arnol′d tongue the algorithm resumes the computation of apparently smooth mesh functions.

4.4. Recursive Construction of the Discretised System. When developing numerical algorithms on multi-dimensional domains one typically introduces a bijective map of the set of multi-indices onto a set of single indices such that the discrete function values can be stored as vectors. Thereby, one obtains a finite-dimensional nonlinear algebraic system. In the following, we present a different approach that not only simplifies the implementation but also allows the computation of tori of arbitrary dimension $p \geq 1$.

Consider the differential equations for tori of increasing dimension $p \geq 0$ written as a root-finding problem in function space:

$$
\begin{aligned}
&\text{0-torus:} && 0 = F^0(u) := f(u)\,, \\
&\text{1-torus:} && 0 = F^1(u) := f(u) - \omega_1 \frac{\partial u}{\partial \theta_1} && = F^0(u) - \omega_1 \frac{\partial u}{\partial \theta_1}\,, \\
&\text{2-torus:} && 0 = F^2(u) := \left(f(u) - \omega_1 \frac{\partial u}{\partial \theta_1} \right) - \omega_2 \frac{\partial u}{\partial \theta_2} && = F^1(u) - \omega_2 \frac{\partial u}{\partial \theta_2}\,, \\
& && \vdots \\
&p\text{-torus:} && 0 = F^p(u) := \left(f(u) - \sum_{i=1}^{p-1} \omega_i \frac{\partial u}{\partial \theta_i} \right) - \omega_p \frac{\partial u}{\partial \theta_p} = F^{p-1}(u) - \omega_p \frac{\partial u}{\partial \theta_p}\,.
\end{aligned}
$$

We observe that the expressions on the right-hand side can be formed recursively. This

motivates the idea of developing an algorithm that constructs the extended discrete system (4.3) by recursion over the dimension p of the torus.

Let $p \geq 1$ and natural numbers $N_1, \ldots, N_p$ be given. Similar to §4.1 we define the discretisation parameter N, the step-sizes h_i, the mesh-size h and the toroidal index-sets $\mathbb{T}_{N_i}$, $i = 1, \ldots, p$. This time, we recursively define the spaces of mesh-functions:

$$\begin{aligned} \mathbb{G}_N^1 &:= \{\, u_N^1 \mid u_N^1 : \mathbb{T}_{N_1}^1 \to \mathbb{R} \,\}\,, \\ \mathbb{G}_N^q &:= \{\, u_N^q \mid u_N^q : \mathbb{T}_{N_q}^1 \to \mathbb{G}_N^{q-1} \,\}\,, \end{aligned}$$

where $q = 2, \ldots, p$ is the recursion parameter. In the space of vector-valued recursive mesh functions $[\, \mathbb{G}_N^q \,]^n$ we define a scalar product

$$\langle\, u_N^q \,,\, v_N^q \,\rangle_{[\, \mathbb{G}_N^q \,]^n} := \sum_{i=1}^{n} \left\langle\, u_{N,i}^q \,,\, v_{N,i}^q \,\right\rangle_{\mathbb{G}_N^q}\,,$$

where we used the scalar product in the space of real-valued recursive mesh functions $\mathbb{G}_N^q$ on the right-hand side, that is,

$$\begin{aligned} \left\langle\, u_{N,i}^1 \,,\, v_{N,i}^1 \,\right\rangle_{\mathbb{G}_N^1} &:= \frac{1}{N_1} \sum_{j=1}^{N_1} u_{N,i}^1(j) v_{N,i}^1(j)\,, \\ \left\langle\, u_{N,i}^q \,,\, v_{N,i}^q \,\right\rangle_{\mathbb{G}_N^q} &:= \frac{1}{N_q} \sum_{j=1}^{N_q} u_{N,i}^q(j) v_{N,i}^q(j)\,. \end{aligned}$$

In the space $[\, \mathbb{G}_N^q \,]^n$ we use the norm which is induced by the scalar product

$$\|u_N^q\|^2_{[\, \mathbb{G}_N^q \,]^n} := \langle\, u_N^q \,,\, u_N^q \,\rangle_{[\, \mathbb{G}_N^q \,]^n}\,.$$

Addition of two mesh-functions and multiplication with a scalar are defined recursively point-wise.

The discretisation operator $P_N : [\, \mathcal{C}^r(\mathbb{T}^p) \,]^n \to [\, \mathbb{G}_N^p \,]^n$ now assumes the form

$$(P_N u)(j_1) \ldots (j_p) := u(j_1 h_1, \ldots, j_p h_p)\,.$$

If we identify $u_N(j_1, \ldots, j_p)$ and $u_N^p(j_1) \ldots (j_p)$ then the spaces $[\, \mathbb{G}_N \,]^n$ and $[\, \mathbb{G}_N^p \,]^n$ are isometric.

One can interpret a mesh-function $u_N^q \in [\, \mathbb{G}_N^q \,]^n$ as a q-dimensional array with elements in $\mathbb{R}^n$, and $u_N^q(j) \in [\, \mathbb{G}_N^{q-1} \,]^n$ as a $(q-1)$-dimensional array with elements in $\mathbb{R}^n$. The recursive definition is yet another way to actually perform the index computation and the notation $u_N^q(j_1) \ldots (j_q)$ is closely related to the recursive indexing of arrays in C and C++. Its main advantage is that an element $u_N^q \in [\, \mathbb{G}_N^q \,]^n$ can be regarded as an object with an index map that has to be defined for one-dimensional indices only, for instance, by operator overloading. Thus, the dimension p of the torus becomes a free parameter in our algorithm and the mesh-functions $u_N^q \in [\, \mathbb{G}_N^q \,]^n$ may be implemented as a template-class with q as a template-parameter.

So far, we have given a recursive definition of mesh-functions. One still needs to show that the function F_N in equation (4.4) as well as its linearisation can be computed recursively. With the above definitions it is straightforward to derive an algorithm for the evaluation of F_N, for example,

$$F_N^p(u_N^p, \omega) := \begin{pmatrix} G_N^p(u_N^p, \omega) \\ b_N^p(u_N^p) \end{pmatrix}\,, \tag{4.10}$$

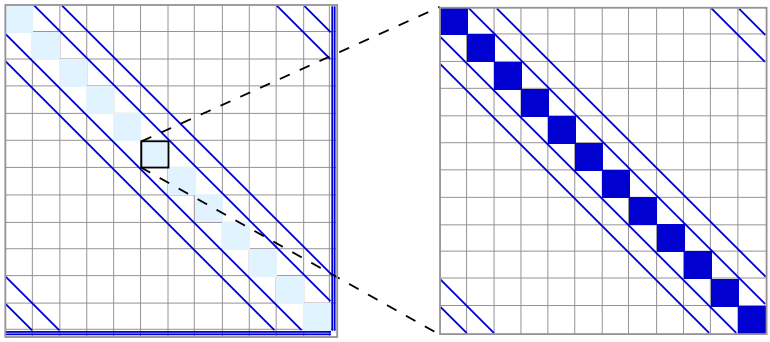

FIGURE 4.3. *Structure of the Jacobian* $(F_N^2)'$ *when using the five-point finite difference formula for* $m = 2$*; see Table 4.1. The blue lines indicate the positions of structural non-zero elements. The light blue diagonal blocks in panel* (a) *are sparse submatrices with a similar structure as the main block in* (a) *as shown in panel* (b)*. The dark blue diagonal blocks in panel* (b) *contain the Jacobians of the right-hand side of the autonomous system (1.1) at the mesh-points.*

where G_N^q contains the recursive discretisation of the partial differential equation that is part of the invariance equation (3.3) :

$$G_N^q(u_N^q,\omega)(j) := \begin{cases} f(u_N^1(j)) - \omega_1(\partial_{N,1}u_N^1)(j) & \text{for} \quad q=1\,, \\ G_N^{q-1}(u_N^q(j),\omega) - \omega_q(\partial_{N,q}u_N^q)(j) & \text{for} \quad q>1\,. \end{cases} \tag{4.11}$$

The term b_N^p represents the discretised phase conditions:

$$b_N^p(u_N^p) := \begin{pmatrix} \langle\, \partial_{N,1}\,\tilde{u}_N^p\,,\; u_N^p\,\rangle \\ \vdots \\ \langle\, \partial_{N,p}\,\tilde{u}_N^p\,,\; u_N^p\,\rangle \end{pmatrix}, \tag{4.12}$$

and the finite-difference approximation $\partial_{N,i}$ of $\frac{\partial}{\partial\theta_i}$ is recursively evaluated as:

$$(\partial_{N,i}u_N^q)(j) := \begin{cases} \dfrac{1}{h_q}\displaystyle\sum_{k=1}^{m}\eta_k\,(\,u_N^q(j+k) - u_N^q(j-k)\,) & \text{for} \quad i=q\,, \\ \partial_{N,i}u_N^q(j) & \text{for} \quad i<q\,. \end{cases} \tag{4.13}$$

Since $[\,\mathbb{G}_N\,]^n$ and $[\,\mathbb{G}_N^p\,]^n$ are isometric, the two equations $F_N(u_N,\omega) = 0$ and $F_N^p(u_N^p,\omega) = 0$ can be regarded as fully equivalent. For efficiency, the finite differences $\partial_{N,i}\,\tilde{u}_N^p$, $i = 1,\ldots,p$, are evaluated only once and normalised to improve the condition of the Jacobian $(F_N^p)'$. This algorithm not only has the advantage that the dimension p of the torus is a free parameter, but the finite-difference formula also appears only in its one-dimensional form at label $i = q$ of (4.13). This remarkably simplifies the implementation of a particular finite-difference scheme as well as its possible substitution by another one.

Next, one derives an algorithm for the recursive evaluation of the Jacobian $(F_N^p)'$ by differentiation of (4.10-4.13). As an additional result we obtain the general structure of this matrix as shown in Fig. 4.3 for the case of a 2-torus where we used the finite-differences for $m = 2$; see Table 4.1. This matrix is a bordered matrix with the

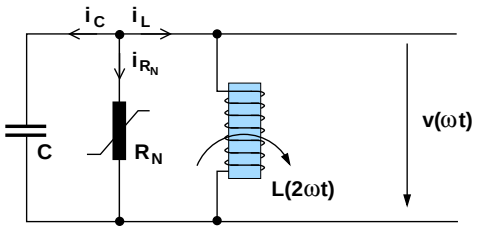

FIGURE 5.1. *A parametrically forced network with a non-linear resistor and a time-dependent inductor as modelled by equation (5.2). The characteristic of the resistor is approximately cubic and has regions with negative slope. The periodic forcing is due to the time-dependence of the inductance.*

principle structure

$$(F_N^p)' = \begin{pmatrix} \dfrac{\partial G_N^p}{\partial u_N^p} & a_N^p \\ b_N^p & 0 \end{pmatrix},$$

where b_N^p is defined as above and the columns of a_N^p contain the partial difference quotients $\partial_{N,i} u_N^p$ for $i = 1, \ldots, p$. Here, (u_N^p, ω) denotes the point of linearisation. One can interpret the main part $\frac{\partial G_N^p}{\partial u_N^p}$ as a recursive block matrix where the structure repeats in the diagonal blocks as indicated in Fig. 4.3 (b).

5. Examples. In this section we demonstrate the performance of our algorithm with two examples arising in nonlinear electrical engineering. First, we extensively investigate a parametrically forced network of Philippow [47] in §5.1. This example is particularly difficult for our algorithm because strong resonances with wide Arnol′d tongues exist in parameter space. Ironically, it was the break-down of our algorithm near strong resonances that gave rise to the more thorough analysis presented here. In addition, it is a typical example for the problems that one may face in order to obtain suitable start data. Namely, the widely used homotopy method [20] to obtain seed solutions for the computation of periodic orbits does not work, because the analytically known solution may be singular. Here, the analytically known torus lies at a branch-point, which means that we cannot initialise a continuation algorithm with this torus. Furthermore, in the two-dimensional parameter space of this example, the torus persists locally as a quasi-periodic or 'weakly resonant' invariant torus in only one direction. If, for a given ODE, one cannot carry out a similar analysis 'by hand', as is typically the case for higher-dimensional ODEs, one relies on simulation data.

Our second example described in §5.2 can be regarded as a typical area of application of our algorithm in its current state of development. The two basic frequencies are of different order of magnitude and, therefore, no strong resonances occur. The invariant tori undergo 'local bifurcations' (see §5.2) and our algorithm has no problems to 'step over' the regions where the tori change stability, as well as to compute the parts of the branches where the tori are of saddle type. One could obtain start data from a torus bifurcation of a periodic orbit, but this is not yet implemented; we used simulation data to obtain a seed solution.

5.1. A Parametrically Forced Electrical Network. As our first example we investigate a nonlinear network arising in electrical engineering, given by Philippow

in [47] and used as a 2:1 frequency divider. The circuit is depicted in Fig. 5.1 and its model equation can be derived as follows. Since it is a shunt circuit the drop of voltage over each element is identical and we denote it by $v(\omega t)$. Applying Kirchhoff's laws we obtain a differential equation from the node equation

$$i_C + i_{R_N} + i_L = 0$$

where the currents i_C, i_{R_N} and i_L, respectively, are given by the formulas

$$\begin{aligned} i_C &= C\frac{dv}{dt}\,, \\ i_{R_N} &= b_1 v^3 - b_2 v\,, \\ i_L &= \frac{\psi}{L_0(1+\frac{b}{2}\sin 2\omega t)} \approx \frac{\psi}{L_0}\left(1-\frac{b}{2}\sin 2\omega t\right)\,. \end{aligned}$$

Using the relation $v = \frac{d\psi}{dt}$ for the inductance and denormalising all quantities one can derive an ODE of the form; see [47],

$$\ddot{x} + \alpha\dot{x}^3 - \beta\dot{x} + (1 + B\sin 2t)x = 0. \tag{5.1}$$

Here, $x \in \mathbb{R}$ is the denormalised voltage and the parameters $\alpha = \varepsilon - B$ and $\beta = \frac{\varepsilon}{2} - B$, where $B, \varepsilon \in \mathbb{R}$, are chosen such that the system response $x(t)$ is an almost harmonic 2π-periodic signal, in other words, the frequency of the input signal is halved.

5.1.1. Qualitative Analysis. In what follows we are going to investigate the qualitative behaviour of solutions of equation (5.1) over a wide range of parameter values and demonstrate the existence of both quasi-periodic and phase-locked invariant tori. We start our investigation with a qualitative analysis of the system for $B = 0$, where no forcing is present. In this case the ODE can be rewritten as the first order system

$$\left\{\begin{array}{rcrcrcl} \dot{x}_1 &=& & & x_2\,, & & \\ \dot{x}_2 &=& -x_1 &+& \frac{\varepsilon}{2}x_2 &-& \varepsilon x_2^3\,. \end{array}\right. \tag{5.2}$$

The bifurcation diagram of (5.2) is given in Fig. 5.2 (a). We immediately see that (5.2) always has the trivial solution $(x_1, x_2) = (0, 0)$ (blue line), which is an equilibrium of the flow, attracting for $\varepsilon < 0$ and repelling for $\varepsilon > 0$. At $\varepsilon = 0$ the equilibrium undergoes a (degenerate) Hopf bifurcation. Namely, system (5.2) becomes the harmonic oscillator

$$\left\{\begin{array}{rcr} \dot{x}_1 &=& x_2\,, \\ \dot{x}_2 &=& -x_1\,, \end{array}\right.$$

and we conclude, that a vertical family of neutrally stable 2π-periodic orbits branches off the family of equilibria (green line).

For further investigation in a neighbourhood of $\varepsilon = 0$, we transform (5.2) into polar coordinates and apply the averaging method [27]. This yields the simple system

$$\left\{\begin{array}{rcl} \dot{r} &=& \frac{\varepsilon}{8}r(2-3r^2)\,, \\ \dot{\theta} &=& 1\,. \end{array}\right.$$

The nontrivial zeroes $r_{1,2} = \pm\sqrt{2/3}$ correspond for small $|\varepsilon|$ to a 2π-periodic orbit of system (5.2) near

$$\{\ r = \sqrt{2/3},\ \theta = t\ \} \quad = \quad \{\ x_1 = \sqrt{2/3}\cos t,\ \ x_2 = -\sqrt{2/3}\sin t\ \},$$

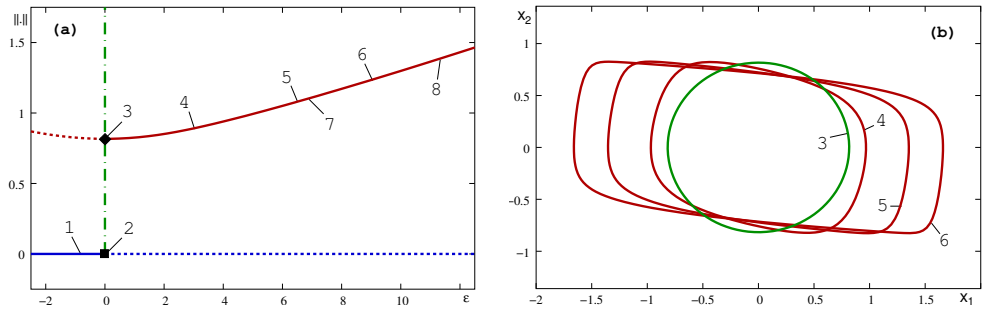

FIGURE 5.2. *The bifurcation diagram of the autonomous system (5.2) depicted as the $\mathcal{L}_2$-norm of the solution versus ε; panel (a). The blue line marked by label 1 is a branch of equilibrium solutions. At label 2, a vertical family of periodic orbits emanates and at label 3 an ε-dependent family γ_ε of periodic orbits branches off the vertical family. The periodic orbits of the family γ_ε for $\varepsilon = 0$ (label 3), $\varepsilon = 3.0$ (label 4), $\varepsilon = 6.5$ (label 5) and $\varepsilon = 9$ (label 6) are plotted in panel (b). Labels 7 and 8 indicate the periodic orbits of γ_ε with period 3π and 4π, which reside on the tip of 1:3 and 1:4 resonance tongues, respectively.*

which is attracting for $\varepsilon > 0$. Therefore, an ε-dependent family γ_ε of periodic orbits (red curve in Fig. 5.2) branches off the vertical family that we found above. In Fig. 5.2 (b) some periodic orbits of γ_ε are shown in phase space.

The fully forced system is the first-order ODE

$$\left\{\begin{array}{rcl} \dot{x_1} &=& x_2 \\ \dot{x_2} &=& -(1 + B\sin\theta)\, x_1 + \dfrac{\varepsilon}{2} x_2 - \varepsilon x_2^3 \\ \dot{\theta} &=& 2, \end{array}\right. \tag{5.3}$$

where $\theta \in \mathbb{T}^1$. For small forcing amplitudes $B > 0$, we can deduce the qualitative behaviour from the results obtained for $B = 0$. Namely, for $B = 0$, an ε-dependent family $T_{\varepsilon,0} := \gamma_\varepsilon \times \mathbb{T}^1$ of invariant tori exists for system (5.3). Since the periodic orbits γ_ε are asymptotically stable for $\varepsilon > 0$ and the flow on $T_{\varepsilon,0}$ is parallel due to decoupling, the tori of $T_{\varepsilon,0}$ are normally hyperbolic. This implies that for sufficiently small $B > 0$ a family $T_{\varepsilon,B}$ of normally hyperbolic invariant tori exists, which are either quasi-periodic or phase-locked, depending on ε. We expect that these invariant tori have cross-sections that are similar to the periodic orbits of the family γ_ε; see Fig. 5.2 (b).

5.1.2. Numerical Analysis. Let $T_1 = \pi$ (so $\omega_1 = 2$) denote the forcing period and $T_2 = 2\pi/\omega_2$ the (ε-dependent) period of an element of γ_ε. Then the rotation number ϱ_ε is defined by $\varrho_\varepsilon := T_1/T_2 = \omega_2/\omega_1$. A resonance tongue in the (ε, B) parameter plane starts at each point $(\varepsilon, 0)$, where ϱ_ε is rational; see Fig. 5.3 (a). For simplicity, we restrict ourselfs to the case of strong resonances, that is, resonances where $\varrho_\varepsilon \in \{1/1,\, 1/2,\, 1/3,\, 1/4\}$. The labels 3, 7 and 8 in Fig. 5.2 (a) mark the points on γ_ε for which the periodic orbits have period $T_2 = 2T_1$, $3T_1$ and $4T_1$, respectively. These periodic orbits reside on the tips of the 1:2, 1:3 and 1:4 resonance tongues at $B = 0$ and $\varepsilon \approx 0$, 6.87, 11.32, respectively. The analysis above showed that $T_2 = 2\pi$ for $\varepsilon = 0$. Hence $\varrho_0 = 1/2$. The values of ε for which $\varrho_\varepsilon \in \{1/3,\, 1/4\}$ were obtained by continuation of γ_ε using AUTO [20].

Fig. 5.3 shows a simplified bifurcation diagram (a) of system (5.3) in the (ε, B)-parameter plane and the bifurcation diagram of the trivial π-periodic orbit $x \equiv 0$ for

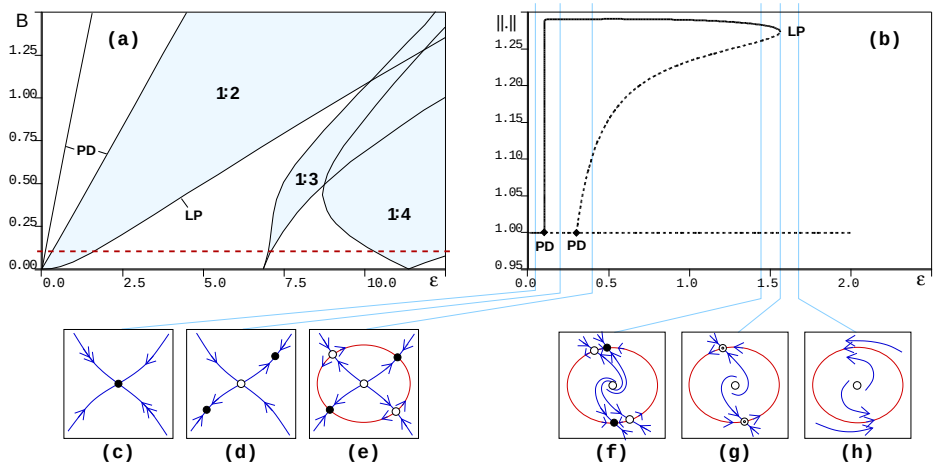

FIGURE 5.3. *Simplified bifurcation diagram of the full system (5.3) in the (ε, B) parameter plane (a). The 1:2, 1:3 and 1:4 resonance tongues are drawn as filled areas. Along the dotted line at $B = 0.1$, we continued the trivial π-periodic orbit and panel (b) shows the corresponding bifurcation diagram. Schematic phase portraits illustrating the changes in the time-π stroboscopic map are shown in the panels (c)-(h).*

$B = 0.1$; panel (b). In addition, the panels (c)-(h) illustrate the qualitative changes in the phase portraits of the period-π stroboscopic map. For small $\varepsilon > 0$ there only exists a trivial fixed point (c). As ε increases, two consecutive period-doubling bifurcations occur at $\varepsilon \approx 0.1$ (d) and at $\varepsilon \approx 0.3$ (e) and two 2-periodic points emerge, one saddle and one node. The fixed point $(0, 0)$, thereby, becomes an unstable node. After the second period-doubling bifurcation a 1:2 phase-locked invariant torus is formed by a saddle-node connection of invariant manifolds of the 2-periodic points (e). At $\varepsilon \approx 1.1$ the Floquet multipliers become complex conjugate and the fixed point is a spiral source (f). At the same time, as $\varepsilon > 0.3$ grows, the 2-periodic points move towards each other and finally merge for $\varepsilon \approx 1.56$ in a saddle-node bifurcation (g) and disappear. For $\varepsilon > 1.56$ we leave the 1:2 resonance tongue and the torus becomes quasi-periodic or weakly resonant (h), depending in a delicate way on ε.

5.1.3. Continuation of Tori. Using the proposed algorithm, we compute the Cantor-like family of quasi-periodic invariant tori for fixed $B = 0.1$ (dashed red line in Fig. 5.3 (a)) that exists in the interval $\varepsilon \in [1.5, 7]$ in between the 1:2 and 1:3 resonance tongues. During the continuation phase-locking will occur, but almost all of the resulting periodic orbits will have such high periods that, numerically, the flow can be regarded as quasi-periodic.

In order to obtain good start data for the continuation of the invariant tori for $B = 0.1$ we use the fact that the perturbed torus $T_{\varepsilon,B}$ for small $B > 0$ is near $T_{\varepsilon,0}$, which is given by the set $\gamma_\varepsilon \times \mathbb{T}^1$. Therefore, we can use an approximation to $T_{\varepsilon,0}$ as the seed for approximating $T_{\varepsilon,B}$. We computed a numerical approximation of the torus for $\varepsilon = 2$ on a 41×101-mesh using Newton's method and the torus function $x_1(\theta_1, \theta_2) = \sin\theta_2$, $x_2(\theta_1, \theta_2) = \cos\theta_2$ together with the basic frequencies $\omega_1 = 2$ and $\omega_2 = 2.08$ as a seed solution. The value $\varepsilon = 2$ is chosen in order to be far enough away from the 1:2 resonance tongue so that we can expect a fast convergence of Newton's method.

Fig. 5.4 shows the invariant tori together with their cross-sections at $\theta_1 = 0$ for

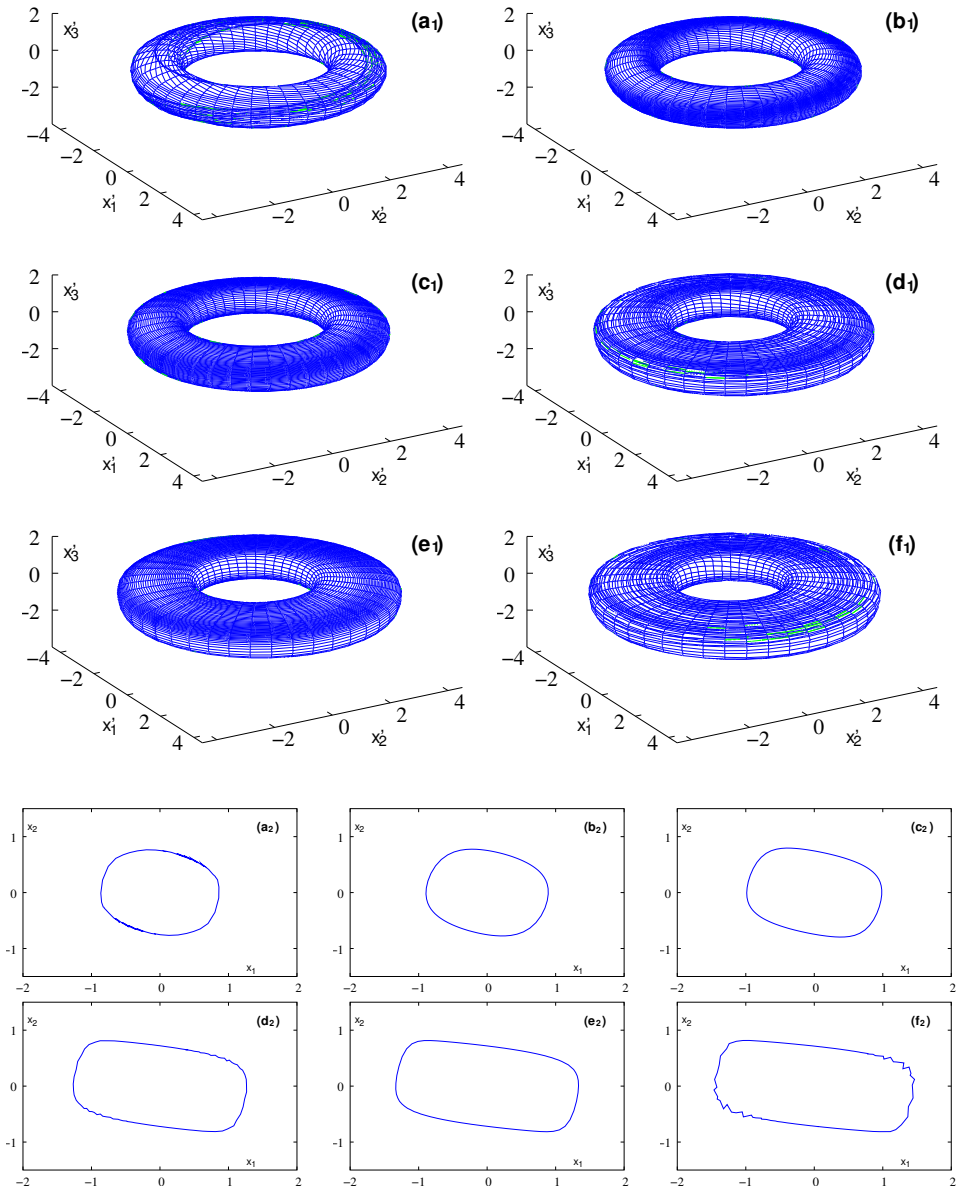

FIGURE 5.4. *The invariant torus of system (5.3) together with cross sections at* $\theta_1 = 0$ *for* $B = 0.1$ *and* $\varepsilon = 1.750$ $(a_1,\ a_2)$, $\varepsilon = 2.000$ $(b_1,\ b_2)$, $\varepsilon = 3.054$ $(c_1,\ c_2)$, $\varepsilon = 5.493$ $(d_1,\ d_2)$, $\varepsilon = 6.000$ $(e_1,\ e_2)$ *and* $\varepsilon = 6.884$ $(f_1,\ f_2)$, *respectively. The tori are embedded into* $\mathbb{R}^3$ *by* $x_1' = 3 + x_1 \cos\theta_1$, $x_2' = 3 + x_1 \sin\theta_1$ *and* $x_3' = x_2$. *Even though it is very hard to see in cross section* (a_2), *the mesh is actually overlapping itself.*

different parameter values ε; compare also the periodic orbits for $B = 0$ in Fig. 5.2 (b). Starting with an approximation at $\varepsilon = 2.0$, shown in panel (b_1), we first continued the torus for $\varepsilon < 2.0$. As ε approaches the border of the 1:2 resonance tongue, the solution develops more and more ripples (see Fig. 5.4 (a_1)), and the estimated error grows rapidly as depicted in Fig. 5.5 (a). We stopped the computation when the estimated

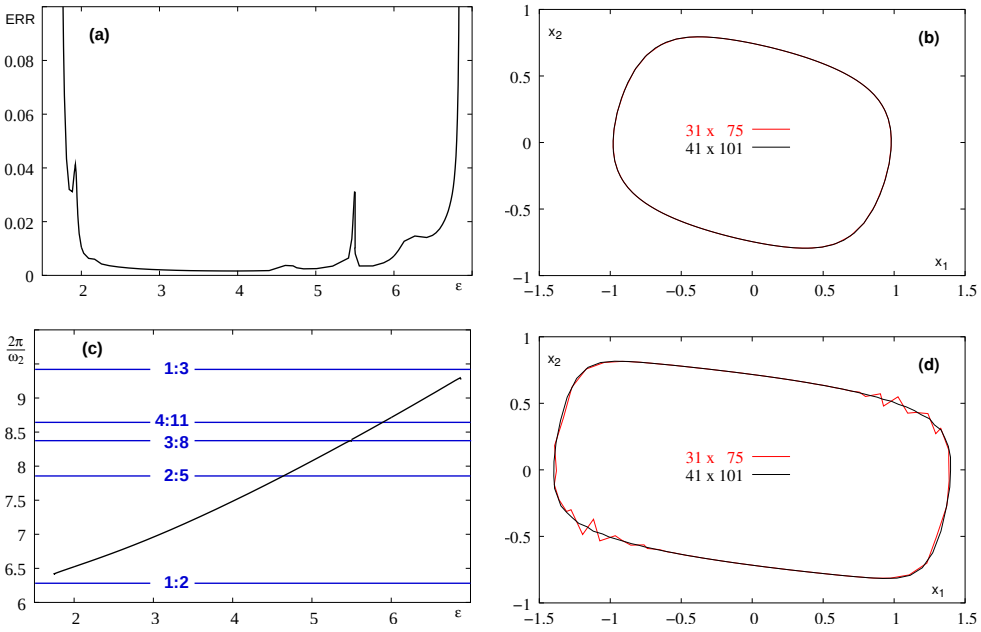

FIGURE 5.5. *Graphs of the estimated error measured via the parameter (see §4.1) on a* 41×101*-mesh (a) and the second period* $T_2 := 2\pi/\omega_2$ *(c) plotted versus* ε*. The horizontal lines in panel (c) indicate selected resonances. Panels (b) and (d) show cross-sections for* $\varepsilon = 3.0$ *(b) and* $\varepsilon = 6.5$ *(d) of solutions on different meshes.*

error became larger than 1. Subsequently, we continued the torus for $\varepsilon > 2$. In the interval $\varepsilon \in [2, 5.4]$ the algorithm converges quickly and the solutions seem smooth, (c_1). For $\varepsilon \approx 5.5$ an 3:8 resonance occurs which influences the algorithm visibly. The estimated error in Fig. 5.5 (a) shows a very clear peak and the approximation is no longer smooth; see Fig. 5.4 (d_1). Furthermore, it takes a large number of continuation steps to pass through the resonance tongue. For $\varepsilon > 5.6$ the algorithm has no problems until the parameter approaches values near the border of the 1:3 resonance tongue at $\varepsilon \approx 7$. We observe the same behaviour as for the 1:2 resonance. Namely, the estimated error grows rapidly and the approximations are again non-smooth; see Fig. 5.4 (f_1).

5.1.4. Performance of the Algorithm. Panels (a) and (c) in Fig. 5.5 illustrate the typical convergence behaviour of our algorithm for a fixed (non-adaptive) mesh and a varying system parameter. The estimated error (a) and, aligned underneath, the second period T_2 (c) are shown as functions of ε; see §4.1 for how the error is measured. The horizontal lines in Fig. 5.5 (c) indicate selected values of T_2 for which resonances occur that affect the computation. Whenever the torus becomes resonant, we expect convergence problems because the torus is then phase-locked and our invariance equation does not hold. But this does not necessarily mean that the algorithm breaks down; see §4.3. Namely, with the exception of the 3:8 resonance, 'weaker resonances' apparently do not influence the algorithm. There is a clear peak in the estimated error around $\varepsilon \approx 5.5$, which is exactly the point where T_2 crosses the 3:8 resonance line, but the algorithm still produces an acceptable approximation; see Fig. 5.4 panels (d_1, d_2). In comparison, the peaks near the 2:5 ($\varepsilon \approx 4.6$) and the 4:11 ($\varepsilon \approx 5.9$) resonances are far less pronounced. Other weak resonances have no observable effects at this numerical accuracy.

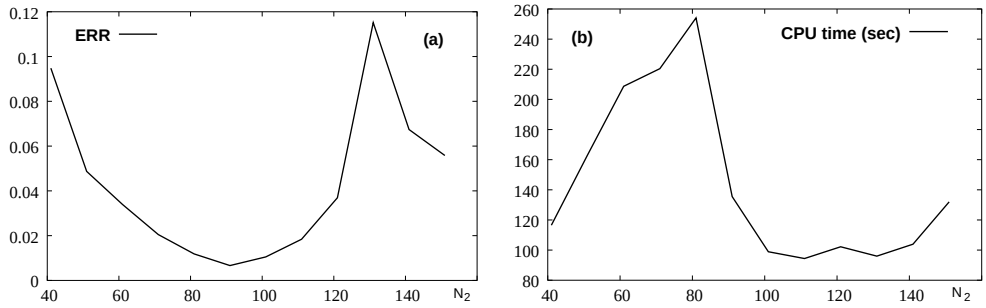

FIGURE 5.6. *Graphical illustration of the computational effort with $N_1 = 41$ fixed and N_2 varying. Panel (a) shows the error estimate versus N_2 and panel (b) the total computation time needed to compute the invariant torus for $\varepsilon = 2$ on an $N_1 \times N_2$-mesh.*

			computation time	
N_2	ERR	fill-in	1 LES	total
41	9.4797e-02	38.2	14.3	116.5
51	4.8700e-02	41.8	20.2	163.1
61	3.3933e-02	42.5	25.8	208.7
71	2.0481e-02	40.1	27.3	220.4
81	1.1848e-02	40.1	31.3	254.1
91	6.6308e-03	28.5	15.5	135.5
101	1.0498e-02	22.1	10.3	98.9
111	1.8392e-02	20.1	10.8	94.4
121	3.6929e-02	20.1	11.7	102.2
131	1.1514e-01	20.2	11.7	96.0
141	6.7397e-02	18.7	10.1	103.9
151	5.5799e-02	19.5	12.0	132.0

TABLE 5.1

Computational effort for $\varepsilon = 2$ and $N_1 \times N_2$ meshes with fixed discretisation parameter $N_1 = 41$ and varying N_2, as shown in the first column. The other columns give the estimated error ERR, the fill-in produced by the ILU preconditioner, the average time (in sec.) for solving one linear equation system (1 LES), and the total computation time (in sec.) for solving the nonlinear discretised equation.

Panels (b) and (d) of Fig. 5.5 show cross sections of the numerical approximation of the torus and illustrate the convergence behaviour of the algorithm for varying (non-adaptive) meshes and fixed parameter values for two typical situations. In panel (b), the parameter value $\varepsilon = 3.0$ is chosen such that the torus is quasi-periodic (or very weakly resonant). In this case we already obtain a good approximation on a coarse mesh. On the other hand, the parameter value $\varepsilon = 6.5$ in panel (d) is close to the 1:3 resonance near $\varepsilon \approx 7$ which clearly results in worse convergence behaviour. Near stronger resonances the cross-sections of approximated tori typically have ripples, as shown on a 31×75 mesh in panel (d). When continuing a torus on a fixed mesh, the amplitude of these ripples grows as the parameter approaches a strong resonance and the algorithm eventually breaks down.

When solving the discretised equations an interesting phenomenon occurs. It turns out that the computation time depends heavily on the proportion N_2/N_1 of the numbers of mesh points. Fig. 5.6 as well as Table 5.1 indicate the computational effort for meshes with $N_1 = 41$ (fixed) mesh points in the θ_1-direction and N_2 (varying) mesh points in the θ_2-direction. The second column of Table 5.1 gives the estimated error ERR, which is also visualised in Fig. 5.6 (a). The next two columns in Table 5.1 give

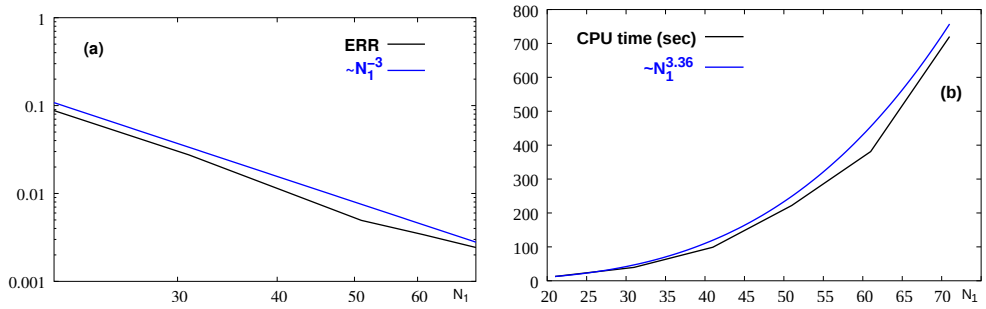

FIGURE 5.7. *The estimated error* (*a*) (*logarithmic scales*) *and the computation-time* (*b*) *as functions of* N_1*, where the choice* $N_2 \approx 2.5N_1$ *is 'optimal'* (*black curves*)*. The estimated error appears to be proportional to* N_1^{-3} (*blue*)*, while the computation time seems to grow proportional to* $N_1^{3.36}$ (*blue*).

the fill-in generated by the ILU preconditioner, (that is, the ratio $\mathrm{nnz}(L+U)/\mathrm{nnz}(A)$, where $\mathrm{nnz}(A)$ is the number of structural non-zero elements of the matrix A) and the average computation time for solving one linear equation system (1 LES). The total computation time for solving the nonlinear discretised system using Newton's method is given in the last column of Table 5.1 and displayed in Fig. 5.6 (b). The results are normalised to 8 Newton Iterations and were obtained using a PC with an 800MHz Pentium III processor and 250MB RAM. The estimated error is minimal for $N_2 = 91$ and the computation time is minimal for $N_2 = 111$. A similar observation can be made for other examples as well and it turns out that there is no obvious correlation with, for instance, the basic frequencies of the approximated torus

Apparently, there exist 'optimal' values for the ratio N_2/N_1 such that for a fixed discretisation parameter $N = \max\{N_1, N_2\}$ the computation time as well as the estimated error become particularly small. Furthermore, for such 'optimal' meshes the ILU preconditioner usually generates a moderate fill-in. Since the system matrices are sparse this implies that storing the incomplete LU-factorisation requires only a moderate amount of memory. For this reason we usually keep the 'optimal' ratio N_2/N_1 fixed for our computations. For the example considered here, the data of Table 5.1 suggests that $N_2/N_1 \approx 2.5$ is a good choice and we used this value in our computations as well as in the comparison of meshes in Figs. 5.5 (b) and (d). At present, we have no explanation for this effect.

Fig. 5.7 (a) shows the growth of the estimated error for 'optimal' meshes with $N_2/N_1 \approx 2.5$ as functions of N_1. The estimated error ERR (black) decreases proportional to N_1^{-3} (blue), which is one order of magnitude better than expected, because the error is estimated for a method of order $q = 2$. Similarly, Fig. 5.7 (b) shows the total computation time as a function of N_1 for meshes with $N_2/N_1 \approx 2.5$. The computation time (black) grows approximately proportional to $N_1^{3.36}$ (blue), which means that doubling N_1 increases the computation time approximately by a factor of 10. The observed time complexity $\mathcal{O}(N_1^{3.36})$ is more than two orders of magnitude less than the worst case $\mathcal{O}(N_1^6)$.

5.2. A circuit with saturable inductors. As our second example we numerically investigate a nonlinear electrical circuit given by Hayashi in [29]. The circuit is depicted in Fig. 5.8 and contains an oscillator built by the two saturable inductors I_1 and I_2, a capacitor C, a resistor R_1 and an AC voltage source S_1. Furthermore, a DC bias is superposed by the loop S_2-R_2-I_1-I_2 where S_2 is a DC voltage source and R_2 a

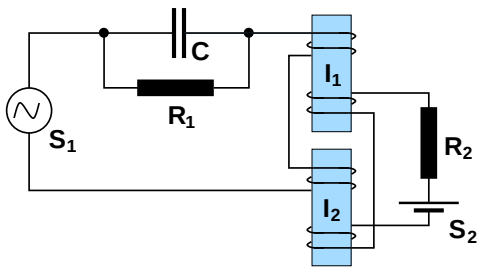

FIGURE 5.8. *The resonant circuit with two saturable inductors (I_1 and I_2) described by system (5.4). In addition, the circuit contains an AC (S_1) and a DC (S_2) voltage source.*

further resistor. The nonlinear characteristics of the cores of I_1 and I_2 are assumed to be cubic and hysteresis is neglected. The ODEs modelling the circuit are

$$\left\{\begin{array}{rcl} \dot{x}_1 &=& x_2\,, \\ \dot{x}_2 &=& -k_1 x_2 - \frac{1}{8}(x_1^2+3x_3^2)x_1 + B\cos t\,, \\ \dot{x}_3 &=& -\frac{1}{8}k_2(3x_1^2+x_3^2)x_3 + B_0\,, \\ \dot{t} &=& 1\,. \end{array}\right. \tag{5.4}$$

Here, $x \in \mathbb{R}^3$ and $B_0, B, k_1, k_2 \in \mathbb{R}$ are free parameters; see [29] and [54] for more details of the derivation. The values of the x_i are dimensionless quantities and do not correspond directly to particular currents or voltages of the circuit. For $x_3 \equiv 0$ and $B_0 = 0$ one obtains Duffing's equation, therefore, system (5.4) is sometimes referred to as being of Duffing type. System (5.4) was studied extensively in, for example, [29] and [54] using simulation and averaging and it was found that quasi-periodic invariant tori and, in particular, a sequence of torus-doubling bifurcations occur.

Let us be more precise by defining the term *torus-doubling bifurcation* in the spirit of Arnéodo, Coullet and Spiegel [1]. Suppose the ODE

$$\dot{x} = f(x,\mu)\,, \qquad f : \mathbb{R}^n \times \mathbb{R} \to \mathbb{R}\,, \tag{5.5}$$

with parameter μ has a periodic orbit that undergoes a period-doubling bifurcation for some $\mu_0 \in \mathbb{R}$. To every periodic orbit of (5.5) we can associate an invariant torus by adjoining the equation

$$\dot{\theta} = \omega\,, \qquad \theta \in \mathbb{T}^1\,. \tag{5.6}$$

The extended system (5.5-5.6) will exhibit a torus-doubling bifurcation at μ_0. Now consider the perturbed system

$$\left\{\begin{array}{rcll} \dot{x} &=& f(x,\mu) &+ \varepsilon g(x,\theta)\,, \\ \dot{\theta} &=& \omega &+ \varepsilon h(x,\theta)\,, \end{array}\right. \tag{5.7}$$

where ε is a positive parameter. For small ε the tori of (5.5-5.6) will persist, provided that these are sufficiently normally hyperbolic. However, at μ_0 these tori lose normal hyperbolicity. Hence, for small $\varepsilon \neq 0$ there exists a whole interval $[\mu_1, \mu_2]$ such that no normally hyperbolic torus exists in (5.7) for $\mu \in [\mu_1, \mu_2]$. For $\mu \notin [\mu_1, \mu_2]$ we still have the situation that on one side of the interval there exist only single tori whereas

on the other side of the interval we have single and double tori. If the length of the interval is small, we refer to this phenomenon as a torus-doubling bifurcation.

It can be shown, that for sufficiently smooth right-hand sides of (5.7) the length of the interval $[\mu_1, \mu_2]$ decreases rapidly with ε, provided that the system can be separated into 'slow' and 'fast' variables; see [42]. This means for quasi-periodic tori that the basic frequencies must have sufficiently distinct values. This condition is met in our example and a crude but simple way to separate 'slow' and 'fast' variables is averaging the system as described below. The sequence of torus doublings mentioned above is observed in simulations of (5.4) for the fixed parameter values $B_0 = 0.03$, $B = 0.22$, $k_2 = 0.05$ and varying $k_1 \in [0.04, 0.2]$. The aim of our investigation is to compute the invariant tori occurring in this system directly as a two-dimensional manifold.

By averaging, it is possible to derive a system that approximates (5.4) and where the variables x and t are decoupled. Suppose the solutions of (5.4) are almost harmonic oscillations with the same frequency as the voltage imposed by the voltage source S_1. Then we may assume that $x(t)$ takes the form

$$\left\{\begin{array}{rcl} x_1(t) &=& y_1(t)\cos t + y_2(t)\sin t\,, \\ x_2(t) &=& -y_1(t)\sin t + y_2(t)\cos t\,, \\ x_3(t) &=& y_3(t)\,, \end{array}\right. \tag{5.8}$$

with time-dependent amplitudes $y \in \mathbb{R}^3$. Using (5.8) one can derive the autonomous system

$$\left\{\begin{array}{rcl} \dot{y}_1 &=& \dfrac{1}{2}(-k_1 y_1 - A y_2)\,, \\ \dot{y}_2 &=& \dfrac{1}{2}(A y_1 - k_1 y_2 + B)\,, \\ \dot{y}_3 &=& B_0 - \dfrac{1}{16}k_2(3r^2 + 2y_3^2)y_3\,, \\ \dot{t} &=& 1\,, \end{array}\right. \tag{5.9}$$

where the 'slow' variables y and the 'fast' variable t are now decoupled; see also [54]. The additional quantities A and r are defined by

$$\begin{array}{rcl} A &:=& 1 - \dfrac{3}{32}(r^2 + 4y_3^2)\,, \\ r^2 &:=& y_1^2 + y_2^2\,. \end{array}$$

5.2.1. Numerical Analysis. The bifurcation diagram of system (5.9) can be computed with AUTO [20]; see Fig. 5.9 (a). The black curve marked by label 1 is a family of equilibrium points. For decreasing $k_1 < 0.2$ the equilibria lose stability at $k_1 \approx 0.1189$ in a Hopf bifurcation (label 2) and a family of attracting periodic orbits branches off (blue). In panel (b) an orbit of this family is shown for $k_1 = 0.09$. At $k_1 \approx 0.0772$ the periodic orbits lose stability in a period-doubling bifurcation (label 4) and a family of doubled periodic orbits emanates. At $k_1 \in \{0.0509, 0.0476, \ldots\}$ further period doublings occur that apparently form a cascade. Orbits of the doubled and quadrupled families are shown in panels (c) and (d) for $k_1 = 0.06$ and $k_1 = 0.05$, respectively.

According to transformation (5.8) an equilibrium point of the averaged system (5.9) corresponds to a periodic orbit of the full system (5.4). Therefore, we expect a

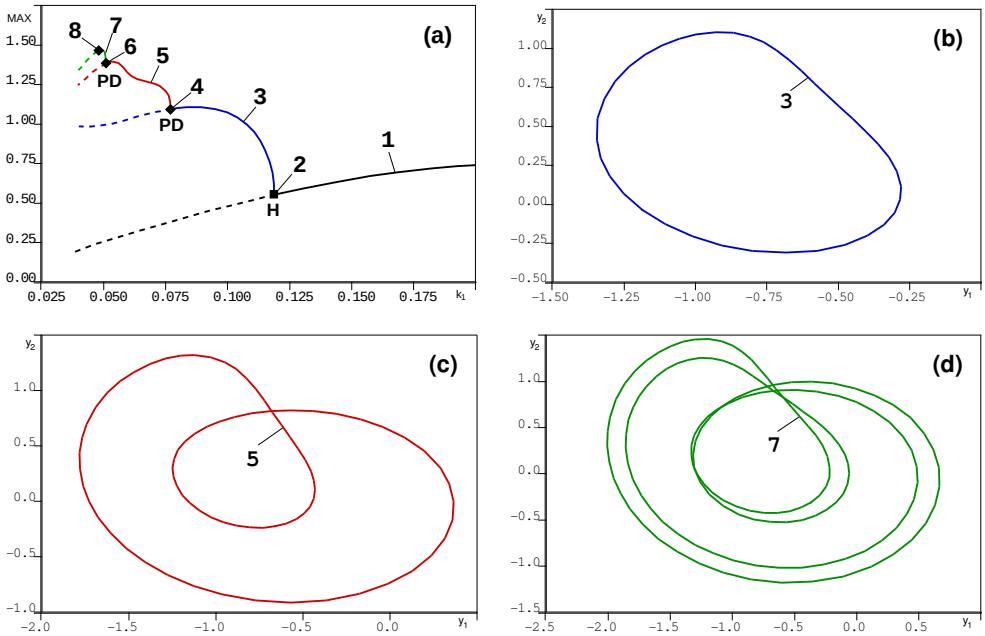

FIGURE 5.9. *The bifurcation diagram of system (5.9) with the maximum of y_2 versus k_1 (a). The black line marked by label 1 is a branch of equilibrium points. For decreasing k_1 a family of periodic orbits (blue) branches off in a Hopf bifurcation at label 2. It seems that for decreasing k_1 a cascade of period-doubling bifurcations occur, the start of which is indicated in panel (a) by the labels 4, 6 and 8. The attracting periodic orbits for $k_1 = 0.09$ (label 3), $k_1 = 0.06$ (label 5) and $k_1 = 0.05$ (label 7) are shown in panels (b), (c) and (d), respectively, projected into the (y_1, y_2)-plane. For $k_1 \approx 0.04$ a strange attractor is observed in simulations.*

family of periodic orbits in the full system (5.4) close to the branch of equilibria of system (5.9). From the occurrence of a Hopf bifurcation at label 2 in the averaged system we conclude that in the full system the family of periodic orbits undergoes a torus bifurcation near $k_1 \approx 0.1189$ and that a family of invariant tori emanates. Similarly, we expect that the period-doubling bifurcations of the averaged system at labels 4, 6, 8, etc. in Fig. 5.9 correspond to torus-doubling bifurcations at 'nearby values' of k_1 in the full system. In fact, in simulations we observe quasi-periodic orbits and a sequence of torus doublings which seems to result in a strange attractor. Moreover, the invariant circles of the period-2π stroboscopic map have a shape similar to the periodic orbits shown in Fig. 5.9 (b)-(c); see also [54].

5.2.2. Continuation of Tori. It is possible to compute the family of periodic orbits (black curve in Fig. 5.10 (a)) of the full system (5.9) with AUTO [20] whereby a torus bifurcation is detected at $k_1 \approx 0.1214$ (label 2). Using our algorithm we can complete this bifurcation diagram by branches of tori (blue and red), including the parts of the branches where the tori are of saddle-type (dashed). Note, that these tori cannot be obtained by simulation. The bifurcation diagram is shown in Fig. 5.10 (a) and the branches are labelled in the same way as in Fig. 5.9 (a). These two bifurcation diagrams appear to be very similar which is numerical evidence that the qualitative analysis using the averaged system (5.9) is accurate for this system and the choice of parameter values.

Fig. 5.11 shows the primary and Fig. 5.12 the doubled tori for different parameter values. The torus in Fig. 5.11 (a) is close to the torus bifurcation and, therefore,

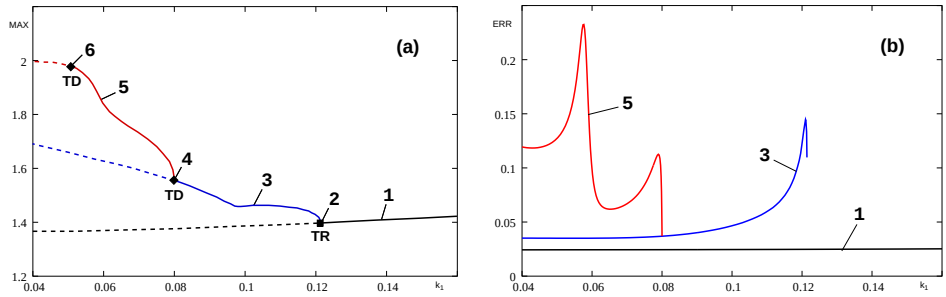

FIGURE 5.10. *The bifurcation diagram of system (5.4) with* $\max_{\theta\in\mathbb{T}^2}\{|u_1(\theta)|,|u_2(\theta)|\}$ *versus* k_1 *(a). The black curve marked by label 1 is a branch of periodic orbits. For decreasing* k_1 *a family of invariant tori (blue, label 3) branches off in a torus bifurcation at* $k_1 \approx 0.1214$ *(label 2). The invariant tori of this family undergo a torus-doubling bifurcation at* $k_1 \approx 0.0799$ *(label 4) and a family of doubled invariant tori emanates (red, label 5). As* k_1 *decreases further, more torus-doubling bifurcations are found, for example at* $k_1 \approx 0.0517$ *(label 6), which seem to form a cascade similar to the cascade of period doublings found in system (5.9). Panel (b) shows the estimated error for each branch of the bifurcation diagram (a), which was monitored as a function of* k_1*.*

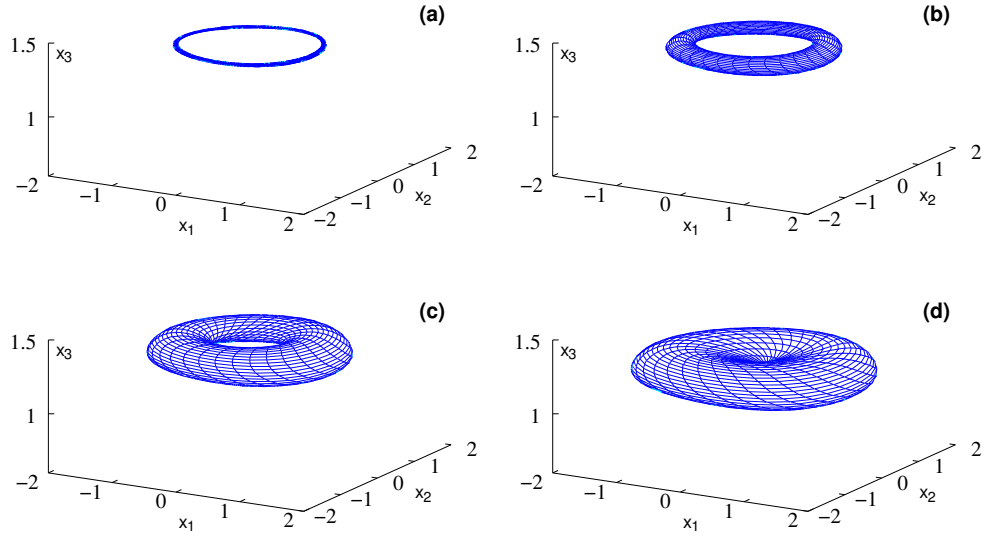

FIGURE 5.11. *The primary invariant torus of system (5.4) for* $k_1 = 0.1214$ *(a),* $k_1 = 0.1182$ *(b),* $k_1 = 0.1044$ *(c), and* $k_1 = 0.0444$ *(d), respectively, projected onto* (x_1, x_2, x_3)*-space. For decreasing* k_1 *the torus separates rapidly from the periodic orbit and becomes 'fatter'. Note that the torus in panel (d) is of saddle type.*

almost coincides with the unstable periodic orbit inside it. In Fig. 5.12 we left out part of the tori and highlighted a cross-section. This cross-section is actually an approximation to the invariant closed curve of the period-2π stroboscopic map of the full system (5.4); see §3. Hence, it is similar to the doubled periodic orbits of the averaged system (5.9); see also Fig. 5.9 (c). The self intersection of the doubled tori is due to the projection of the tori from the 4-dimensional phase space $\mathbb{R}^3 \times \mathbb{T}^1$ into the 3-dimensional (x_1, x_2, x_3)-space, which is also a Poincaré section of the phase space for fixed $\theta \in \mathbb{T}^1$.

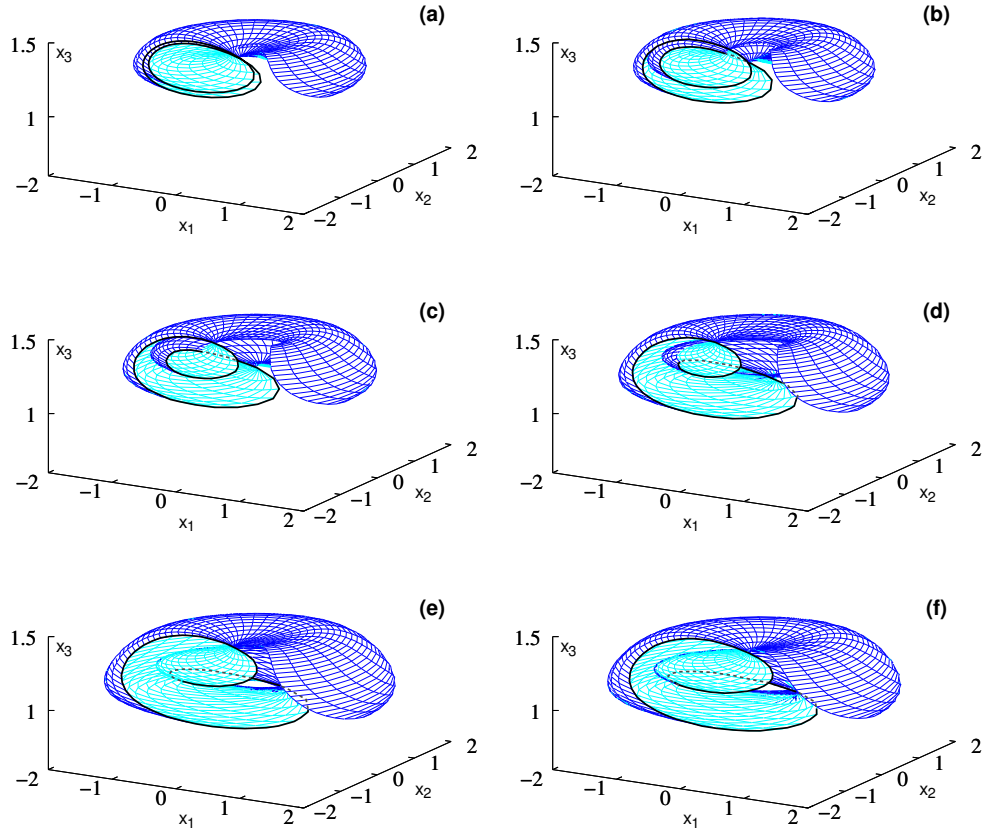

FIGURE 5.12. *The doubled invariant torus of system (5.4) for $k_1 = 0.0797$ (a), $k_1 = 0.0775$ (b), $k_1 = 0.0700$ (c), $k_1 = 0.0598$ (d), $k_1 = 0.0502$ (e), and $k_1 = 0.0421$ (f), respectively, projected onto (x_1, x_2, x_3)-space. Only part of the tori is shown and a cross-section is drawn as a black curve to emphasise the evolution of the tori. The behaviour of the cross-section is qualitatively similar to the behaviour observed in period-doubling bifurcations of periodic orbits. Note that the tori shown in panels (e) and (f) are of saddle type. The self intersection of the tori is due to projection.*

5.2.3. Performance of the Algorithm. The branches of invariant tori were computed as follows. We obtained seed approximations of the primary and doubled invariant tori by two dimensional Fourier analysis of simulation data obtained for $k_1 = 0.09$ (primary torus) and $k_1 = 0.0775$ (doubled torus), respectively, and continued the branches in both directions. The tori were computed on a 31×31 mesh (primary torus) and a 31×61 mesh (double torus), respectively. Unlike the previous example, we do not encounter convergence problems caused by strong resonances because the rotation numbers vary between $\rho_{k_1} \in [0.093, 0.132]$ for the primary tori and $\rho_{k_1} \in [0.053, 0.074]$ for the doubled tori. The parameter values at which the torus-doubling bifurcations occur were obtained by investigation of the simulation as well as the continuation data.

The convergence behaviour of our algorithm depending on the parameter is illustrated in Fig. 5.10 (b). It shows the graphs of the estimated error along each branch as functions of the parameter k_1. The error remains bounded and the occurring peaks are not high compared to the average error of each branch. The error is relatively large, but this is due to the coarse meshes used; the solutions themselves seem smooth for all parameter values.

6. Conclusion. In this paper, we derived an invariance equation for quasi-periodic invariant tori that gives rise to a natural parametrisation of tori under the assumption that the flow on these tori is quasi-periodic. The discretisation of the invariance equation by central finite-differences led to algorithms of high order of consistency. A proof of stability was given in the case that the ODE is available in partitioned form. The algorithm is implemented as a corrector in a one-parameter continuation environment and computes invariant tori with prescribed accuracy even when the tori are not quasi-periodic, provided the resonances encountered are 'weak enough'. This was shown with examples. Furthermore, the algorithm is able to 'step over' regions where the torus changes stability, as was demonstrated in the last example.

In future work we plan to implement algorithms that can start a continuation from a local torus (Neimark-Sacker) bifurcation that is detected during the continuation of a periodic orbit. We also intend to implement the detection of 'local torus bifurcations' and branch switching. This will be based on the detection of bifurcations of the cross-sections of invariant tori similar to the detection of local bifurcations of periodic orbits.

The main weakness of our approach as a general tool for continuation of tori is its derivation based on the assumption of quasi-periodicity. At first, this may seem a greatly restrictive assumption. However, as reviewed in §2, there are similar restrictive (but distinct) assumptions inherent in all previous approaches. Also, as we have seen, the method works in practice away from 'too strong resonances'. Future work will address this weakness directly. One idea is to locally modify the vectorfield such that the flow on the torus is diffeomorphic to a parallel flow and the torus as a geometric object is invariant under the original flow. Future work will also consider a rigorous proof of stability.

7. Acknowledgements. The authors would like to thank Bernd Krauskopf and Alan Champneys for their careful reading of and constructive suggestions on a draft of this manuscript. Considerable credit goes to them and also to Jan Sieber for inspiring discussions and valuable hints. This work was supported by EPSRC grant GR/R72020/01.

REFERENCES

[1] A. Arnéodo, P.H. Coullet and E.A. Spiegel, *Cascade of period doublings of tori*, Phys. Lett. A 94, 1 (1983), pp. 1–6.

[2] V.I. Arnol′d, *Small denominators. I. Mappings of the circumference to itself*, Izv. Akad. Nauk SSSR, Ser. Mat., 26 (1961), pp. 21–86; English translation, Amer. Math. Soc. Transl., 46 (1965), pp. 213–284.

[3] S. Bauer, O. Brox, J. Kreissl, B. Sartorius, M. Radziunas, J. Sieber, H.J. Wünsche and F. Henneberger, *Nonlinear dynamics of semiconductor lasers with active optical feedback*, Physical Review E, 69 (2004), 016206.

[4] K. Bernet and W. Vogt, *Anwendung finiter Differenzenverfahren zur direkten Bestimmung invarianter Tori*, ZAMM, 74(6) (1994), pp. T577–T579.

[5] P. Bonello, M.J. Brennan and R. Holmes, *Non-linear modelling of rotor dynamic systems with squeeze film dampers — an efficient integrated approach*, J. Sound and Vib., 249(4) 2002, pp. 743–773.

[6] H.W. Broer, *Quasi-periodic bifurcations, applications*, Proceedings of the XIth Congress on Differential Equations and Applications/First Congress on Applied Mathematics (Spanish) (Ma'laga, 1989), pp. 3–21, Univ. Ma'laga, Ma'laga, 1990.

[7] H.W. Broer, A. Hagen, and G. Vegter, *Multiple purpose algorithms for invariant manifolds*, Second International Conference on Dynamics of Continuous, Discrete and Impulsive Systems (London, ON, 2001). Dyn. Contin. Discrete Impuls. Syst. Ser. B Appl. Algorithms 10(1-3), 2003, pp. 331–344.

[8] H.W. Broer, G.B. Huitema and M.B. Sevryuk, *Quasi-Periodic Motions in Families of Dynamical Systems*, Springer-Verlag Berlin, 1996.
[9] H.W. Broer, G.B. Huitema, F. Takens and B.L.J. Braaksma, *Unfoldings and bifurcations of quasi-periodic tori*, Mem. Amer. Math. Soc. 83(421) (1990), viii+175 pp.
[10] H.W. Broer, H.M. Osinga and G. Vegter, *Computing a normally hyperbolic invariant manifold of saddle type*, in G.S. Ladde and M. Sambandham, eds., Proceedings of Dynamic Systems & Applications 2, Dynamic Publishers, 1996, pp. 83–90.
[11] ———, *On the computation of normally hyperbolic invariant manifolds*, in H.W. Broer, S.A. van Gils, I. Hoveijn and F. Takens, eds., Nonlinear Dynamical Systems and Chaos, Progress in Nonlinear Differential Equations and Their Applications 19, Birkhäuser Verlag, Basel / Switzerland, 1996, pp. 423–447.
[12] ———, *Algorithms for computing normally hyperbolic invariant manifolds*, Z. angew. Math. Phys., 48(3) (1997), pp. 480–524.
[13] ———, *Computing a normally attracting invariant manifold of a Poincaré map*, in P.L. Butzer, H.Th. Jongen, and W. Oberschelp, eds., Charlemagne and His Heritage, 1200 Years of Civilization and Science in Europe, Volume 2: Mathematical Arts, Brepols Publishers, 1998, pp. 541–549.
[14] W.G. Büntig and W. Vogt, *Numerical Bifurcation Analysis of Nonlinear Power Systems*, Proceedings of the 48th Internationales Wiss. Kolloquium, Technische Universität Ilmenau, 22.-25.9.2003, pp. 373–374.
[15] L.O. Chua and A. Ushida, *Algorithms for computing almost periodic steady-state response of nonlinear systems to multiple input frequencies*, IEEE Trans. Circuits and Systems, 28(10) (1981), pp. 953–971.
[16] L. Debraux, *Numerical computation of a branch of invariant circles starting at a Hopf bifurcation point*, Contemp. Math., 172 (1994), pp. 169–184.
[17] L. Dieci, J. Lorenz and R.D. Russell, *Numerical calculation of invariant tori*, SIAM J. Sci. Stat. Comput., 12 (1991), pp. 607–647.
[18] L. Dieci and J. Lorenz, *Block M-matrices and computation of invariant tori*, SIAM J. Sci. Stat. Comput., 13 (1992), pp. 885–903.
[19] ———, *Computation of invariant tori by the method of characteristics*, SIAM J. Num. Anal., 32(5) (1995), pp. 1436–1474.
[20] E.J. Doedel, A.R. Champneys, Th.F. Fairgrieve, Y.A. Kuznetsov, B. Sandstede and X. Wang, *AUTO 97*: *Continuation and Bifurcation Software for Ordinary Differential Equations* (*with HomCont*), 1997
[21] E.J. Doedel, W. Govaerts, Y.A. Kuznetsov, Computation of periodic solution bifurcations in ODEs using bordered systems, SIAM J. Numer. Anal., 41(2) (2003), pp. 401–435.
[22] K.D. Edoh, R.D. Russell and W. Sun, *Computation of invariant tori by orthogonal collocation*, Applied Numerical Mathematics, 32 (2000), pp. 273–289.
[23] L.C. Evans, *Partial Differential Equations*, American Mathematical Society, Providence, Rhode Island, 1998.
[24] N. Fenichel *Persistence and smoothness of invariant manifolds for flows*, Indiana Univ. Math. J., 21 (1971), pp 193–226.
[25] T. Ge and A.Y.T. Leung, *Construction of invariant torus using Toeplitz Jacobian matrices/fast Fourier transform approach*, Nonlinear Dynamics, 15 (1998), pp. 283–305.
[26] J.A. Glazier and A. Libchaber, *Quasi-periodicity and dynamical systems*: *An experimentalists view*, IEEE Trans. Circ. Sys., 35(7) (1988), pp. 790–809.
[27] J. Guckenheimer and P. Holmes, *Nonlinear Oscillations, Dynamical Systems and Bifurcation of Vector Fields*, Springer-Verlag Berlin, 1997.
[28] W. Hackbusch, *Elliptic Differential Equations*, *Theory and Numerical Treatment*, Teubner Verlag Stuttgart, 1987; English translation, Springer Verlag Berlin Heidelberg, 1992.
[29] C. Hayashi, *Quasi-periodic oscillations in non-linear control systems*, in Selected Papers on Nonlinear Oscillations, Chihiro Hayashi, Professor Emeritus, Kyoto University; Kyoto University 1975, Printed by Nippon Printing and Publishing Company, Ltd. Yoshino, Fukushima-ku, Osaka, Japan.
[30] M. Hermann, *Numerische Mathematik*, R. Oldenbourg Verlag, Munich, 2001.
[31] M.W. Hirsch, C.C. Pugh, M. Shub, *Invariant manifolds*, Lecture Notes in Mathematics, Vol. 583. Springer-Verlag Berlin-New York, 1977.
[32] W. Ji and V. Venkatasubramanian, *Dynamics of a minimal power system*: *invariant tori and quasi-periodic motions*, IEEE Trans. Circuits Systems I Fund. Theory Appl., 42(12) (1995), pp. 981–1000.
[33] Chr. Kaas-Petersen, *Computation of quasiperiodic solutions of forced dissipative systems*, J. Comput. Phys., 58(3) (1985), pp. 395–408.

[34] ———, *Computation of quasiperiodic solutions of forced dissipative systems. II*, J. Comput. Phys., 64(2) (1986), pp. 433–442.

[35] ———, *Computation, continuation, and bifurcation of torus solutions for dissipative maps and ordinary differential equations*, Phys. D, 25(1-3) (1987), pp. 288–306.

[36] I.G. Kevrekidis, R. Aris, L.D. Schmidt and S. Pelikan, *Numerical computations of invariant circles of maps*, Physica D, 16 (1985), pp. 243–251.

[37] B. Krauskopf, N. Tollenaar and D. Lenstra, *Tori and their bifurcations in an optically injected semiconductor laser*, Optics Communications, 156(1-3) (1998), pp. 158–169.

[38] B. Krauskopf, S.M. Wieczorek and D. Lenstra, *Different types of chaos in an optically injected semiconductor laser*, Applied Physics Letters, 77(11) (2000), pp. 1611–1613.

[39] P. Lenas, N.A. Thomopoulos, D.V. Vayenas and S. Pavlou, *Oscillations of two competing microbial populations in configurations of two interconnected chemostats*, Math. Biosci., 148(1) (1998), pp. 43–63.

[40] H. Mingyou, T. Küpper and N. Masbaum, *Computation of invariant tori by the Fourier methods*, SIAM J. Sci. Comput., 18 (1997), pp. 918–942.

[41] G. Moore, *Computation and parametrisation of invariant curves and tori*, SIAM J. of Numer. Anal., 33(6) (1996), pp. 2333–2358.

[42] A.I. Neishtadt, *The separation of motions in systems with rapidly rotating phase*, J. Appl. Math. Mech., 48(2) (1985), pp. 133–139; translated from Prikl. Mat. Mekh., 48(2) (1984), pp. 197–204 (Russian).

[43] N. Nicolaisen, B. Werner, *Discretisation of circle maps*, Z. Angew. Math. Phys., 49(6) (1998). pp. 869–895.

[44] H. Osinga: Computing Invariant Manifolds: Variations on the Graph Transform, Diss., Univ. Groningen, 1996.

[45] S. Östlund, D. Rand, J. Sethna and E. Siggia, *Universal properties of the transition from quasiperiodicity to chaos in dissipative systems*, Phys. D, 8(3) (1983), pp. 303–342.

[46] T.S. Parker and L.O. Chua, *Practical Numerical Algorithms for Chaotic Systems*, Springer-Verlag New York, 1989.

[47] E. Philippow and W.G. Büntig, *Analyse nichtlinearer dynamischer Systeme der Elektrotechnik*: *Einführung in die numerische Untersuchung einfacher Systeme*, Carl Hanser Verlag München et al., 1992.

[48] V. Reichelt, *Computing invariant tori and circles in dynamical systems*, in E.J. Doedel and L.S. Tuckermann, eds., Numerical Methods for Bifurcation Problems and Large-Scale Dynamical Systems, IMA Volumes in Mathematics and its Applications 119 pp. 407–437, Springer Verlag, 2000.

[49] A.M. Samoilenko, *Elements of the Mathematical Theory of Multi-Frequency Oscillations*, Isdatelstvo Nauka, Moskva 1987; English translation, Kluwer Academic Publishers, Dordrecht et al., 1991.

[50] F. Schilder, *TorCont: computation and continuation of quasi-periodic invariant tori*, software package, `http://www.mathematik.tu-ilmenau.de/~fschild/`.

[51] M. van Veldhuizen, *A new algorithm for the numerical approximation of an invariant curve*, SIAM J. Sci. Stat. Comput., 8 (1987), pp. 951–962.

[52] ———, *Convergence results for invariant curve algorithms*, Math. Comp., 51(184) (1988), pp. 677–697.

[53] S. Wiggins, *Normally Hyperbolic Invariant Manifolds in Dynamical Systems*, Springer-Verlag, 1994.

[54] T. Yoshinaga and H. Kawakami, *Bifurcations and chaotic state in forced oscillatory circuits containing saturable inductors*, In: T. Carroll and L. Pecora, Nonlinear Dynamics In Circuits, pp. 89–118, World Scientific Publishing, 1995.